AGU PUBLICATIONS

Tectonics

RESEARCH ARTICLE
10.1002/2013TC003424

Key Points:
- Oligo-Miocene basin fill recorded flexural subsidence during Andean shortening
- Detrital zircon U-Pb and apatite (U-Th)/He results show deformation advance
- Rapid, large-scale exhumation of central Precordillera thrust belt at 12–9 Ma

Supporting Information:
- Readme
- Table S1
- Table S2
- Table S3
- Figure S1a
- Figure S1b
- Figure S1c
- Figure S2
- Figure S3

Correspondence to:
M. Levina,
mariya.levina@gmail.com

Citation:
Levina, M., B. K. Horton, F. Fuentes, and D. F. Stockli (2014), Cenozoic sedimentation and exhumation of the foreland basin system preserved in the Precordillera thrust belt (31–32°S), southern central Andes, Argentina, *Tectonics*, *33*, 1659–1680, doi:10.1002/2013TC003424.

Received 10 AUG 2013
Accepted 14 AUG 2014
Accepted article online 21 AUG 2014
Published online 10 SEP 2014

Cenozoic sedimentation and exhumation of the foreland basin system preserved in the Precordillera thrust belt (31–32°S), southern central Andes, Argentina

Mariya Levina[1], Brian K. Horton[1,2], Facundo Fuentes[3], and Daniel F. Stockli[1]

[1]Department of Geological Sciences, Jackson School of Geosciences, University of Texas at Austin, Austin, Texas, USA, [2]Institute for Geophysics, Jackson School of Geosciences, University of Texas at Austin, Austin, Texas, USA, [3]Pluspetrol, Buenos Aires, Argentina

Abstract Andean retroarc compression associated with subduction and shallowing of the oceanic Nazca plate resulted in thin-skinned thrusting that partitioned and uplifted Cenozoic foreland basin fill in the Precordillera of west-central Argentina. Evolution of the central segment of the Precordillera fold-thrust belt is informed by new analyses of clastic nonmarine deposits now preserved in three intermontane regions between major east directed thrust faults. We focus on uppermost Oligocene-Miocene basin fill in the axial to frontal Precordillera at 31–32°S along the Río San Juan (Albarracín and Pachaco sections) and the flank of one of the leading thrust structures (Talacasto section). The three successions record hinterland construction of the Frontal Cordillera, regional arc volcanism, and initial exhumation of Precordillera thrust sheets. Provenance changes recorded by detrital zircon U-Pb age populations suggest that initial shortening in the Frontal Cordillera coincided with an early Miocene shift from eolian to fluvial accumulation in the adjacent foreland basin. Upward coarsening of fluvial deposits and increased proportions of Paleozoic clasts reflect cratonward (eastward) advance of deformation into the Precordillera and resultant structural fragmentation of the foreland basin into isolated intermontane segments. Apatite (U-Th)/He thermochronometry of basin fill constrains to 12–9 Ma the most probable age of uplift-induced exhumation and cooling of Precordillera thrust sheets. This apparent pulse of exhumation is evident in each succession, suggestive of rapid, large-scale exhumation by synchronous thrusting above a single décollement linking major structures of the Precordillera.

1. Introduction

The Argentine Precordillera of the southern central Andes (28–33°S) forms a N trending fold-thrust belt between the Frontal Cordillera in the western hinterland and basement ranges of the Sierras Pampeanas in the eastern foreland (Figure 1). Cenozoic uplift has been linked to the eastward advance of shortening during progressive shallowing of the subducting Nazca plate [*Jordan et al.*, 1983; *Cahill and Isacks*, 1992; *Ramos*, 2009; *Ramos and Folguera*, 2009]. Whereas the northern Precordillera remains one of the best-understood thrust belts and foreland basin systems on Earth [e.g., *Johnson et al.*, 1986; *Damanti*, 1993; *Jordan et al.*, 1993, 2001; *Jordan*, 1995; *Zapata and Allmendinger*, 1996a, 1996b], the detailed records of the central and southern segments of the Precordillera thrust system and associated contractional basins [*Kley et al.*, 1999; *Vergés et al.*, 2001; *Ramos et al.*, 2002; *Alonso et al.*, 2005] remain relatively poorly constrained within the past 5–20 Myr.

Ramos et al. [2002] outlined several stages of Cenozoic deformation and slab evolution in this segment of the Andes. At 32°S (Figure 1), this history involved ~12–10 Ma subduction of the aseismic Juan Fernández Ridge, a potential driver of slab flattening [*Jordan et al.*, 1993; *Cristallini and Ramos*, 2000; *Yáñez et al.*, 2001; *Kay and Mpodozis*, 2002], 9–6 Ma uplift of the Frontal Cordillera, and sequential thrusting within the Precordillera focused at 5–2 Ma. On the basis of available ages of magmatism and deformation [e.g., *Jordan et al.*, 1997, 2001; *Irigoyen et al.*, 2000], the Precordillera evolved asynchronously, with early to middle Miocene shortening in the north (28–30°S) and Plio-Pleistocene shortening at the southern tip (33–34°S), potentially consistent with southward migration of the subducted Juan Fernández ridge [*Ramos et al.*, 2002].

In the northern Precordillera (Figure 1), multiple studies have linked the detailed Mio-Pliocene accumulation history of the Bermejo foreland basin with ~20 Ma to present shortening of the thrust belt [*Beer and Jordan*, 1989; *Jordan et al.*, 1993, 1997, 2001; *Milana et al.*, 2003]. However, these high-resolution studies underscore

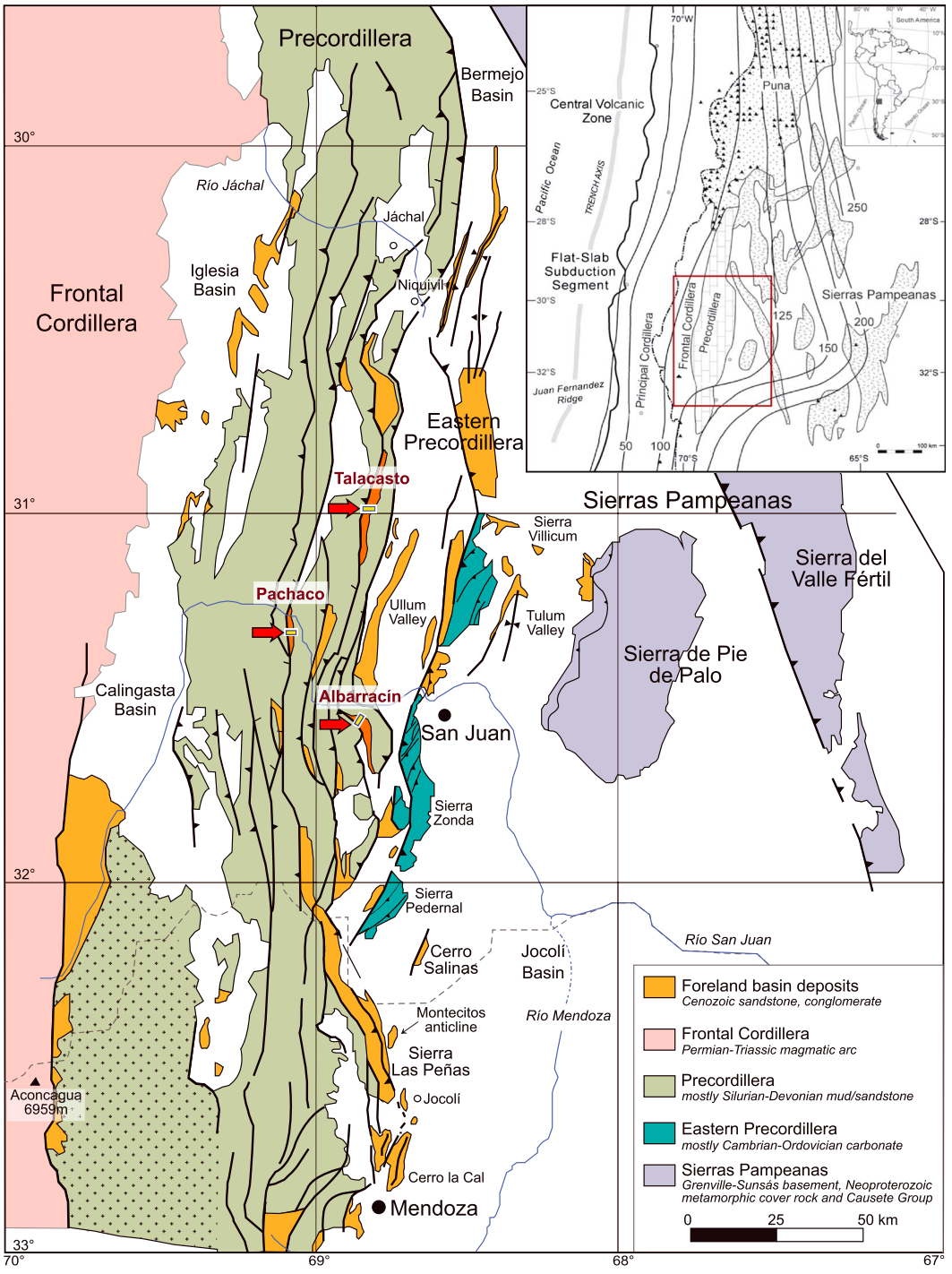

Figure 1. Geologic map of the Precordillera thrust belt and flanking Frontal Cordillera (west) and Sierras Pampeanas (east), with Cenozoic foreland basin deposits shown in orange [after *Vergés et al.*, 2007]. The Pachaco, Talacasto, and Albarracín basin segments are labeled, showing measured section locations (red arrows pointing to small yellow lines). Inset in upper right shows a regional map of the Pampean flat-slab segment of the southern central Andes [after *Ramos et al.*, 2002] with the subducted Nazca plate denoted by depth contours (thin black lines with depth values in kilometers) [after *Cahill and Isacks*, 1992].

major uncertainties in reconstructing the central to southern Precordillera, where limited data are available from selected intermontane basin segments that have not been conclusively correlated [*Milana et al.*, 1993; *Vergés et al.*, 2001]. For example, it remains unclear whether Cenozoic basin fill now exposed in intermontane settings developed as piggyback or wedge-top basins on top of an actively

deforming thrust belt [e.g., *Horton*, 1998; *Echavarria et al*., 2003] or as a once-contiguous foreland basin that was structurally partitioned by subsequent thin-skinned deformation [e.g., *Jordan and Alonso*, 1987; *Horton*, 2005; *Siks and Horton*, 2011].

Our study combines field-based sedimentological analyses with geochronologic and thermochronologic data to provide a refined history of upper crustal deformation, exhumation, and basin development in the central (Río San Juan) segment of the Precordillera at 31–32°S. We present sedimentological observations of Oligo-Miocene basin fill of foreland to intermontane affinity that are preserved in different thrust sheets and laterally distributed along strike within the thrust belt (Figure 1). We are able to constrain the depositional ages and provenance of these sediments using new detrital zircon U-Pb data, which further allow us to spatially correlate the Pachaco, Talacasto, and Albarracín successions, resulting in a protracted history of foreland basin sedimentation and structural partitioning. Finally, we apply apatite (U-Th)/He thermochronometry to better determine the timing of exhumational cooling of basin fill and arrive at a more complete understanding of Precordillera thrust belt evolution.

2. Geologic Setting

The Argentine Precordillera (Figure 1) is a thin-skinned, east vergent thrust belt involving Paleozoic strata and narrow, discontinuous slivers of Cenozoic basin fill deposited in foreland to intermontane settings [*Ramos*, 1999; *Ramos et al*., 1986; *Vergés et al*., 2001]. Over 100 km of E-W shortening has been accommodated by a series of stacked imbricate thrust sheets above a basal decollément [*Allmendinger et al*., 1990; *Von Gosen*, 1992; *Cristallini and Ramos*, 2000]. Cenozoic rocks are preserved in the footwalls of major thrust faults [*Alonso*, 2005; *Jordan et al*., 1993] and preferentially eroded to form N trending intermontane valleys between thrust-generated ranges. The arid climate and limited vegetation promote continuous exposures of clastic basin fill, from basal unconformable contacts with Paleozoic strata to upper fault contacts with overriding thrust sheets. Near the Río San Juan, Cenozoic rocks are exposed near Pachaco, Mogote Cortadera, Río Uruguay, Sierra Talacasto, Pampa Bachongo, Quebrada Albarracín, and along the Ullúm Valley. We focus on nonmarine successions exposed at the Pachaco, Talacasto, and Albarracín localities (Figure 1; see Figure S1 in the supporting information available at doi:10.1002/2013TC003424), which span the axial to eastern front of the Precordillera (69.1–68.8°W). Although recent dam construction along the Río San Juan has limited access between Pachaco and Albarracín, the selected localities provide adequate spatial and temporal coverages for the segmented basin system.

In the axial Precordillera, the Pachaco succession is exposed in a N striking, W dipping panel about 12 km long and 1.5 km wide, south of Pachaco, where the N flowing El Palque creek joins the Río San Juan (Figures 1 and S1a). The base of this section, which unconformably overlies the Devonian Punta Negra Formation of the Sierra de la Cantera to the east, has been estimated at 18–21 Ma on the basis of fossil palynomorphs [*Milana et al*., 1993]. The southernmost Pachaco succession is gently folded into an asymmetric NW plunging syncline, exposing the youngest basin fill in a zone (~7 km upstream of the El Palque-San Juan confluence) truncated by a W dipping thrust fault carrying Paleozoic marine strata.

The Talacasto succession of the eastern Precordillera is exposed ~50 km NE of Pachaco, closer to the eastern deformation front (Figures 1 and S1b). Poorly consolidated Neogene rocks at this locality form a ~3 km wide outcrop belt in a low-relief badlands landscape between the Sierra Talacasto to the east and Sierra de la Crucecita to the west. This ~1000 m thick, W dipping succession is best exposed in gullies beneath low-relief Quaternary alluvial terraces rich in Paleozoic clasts. Upper stratigraphic levels are expressed in the west as a zone of highly deformed basin fill in the footwall of the thrust structure forming the Sierra de la Crucecita.

The Albarracín succession is preserved in the eastern Precordillera along the Río Albarracín, a tributary to the Río San Juan near the Punta Negra Dam (Figures 1 and S1c). Neogene strata cap Paleozoic rocks forming a frontal Precordillera thrust sheet and associated range, the Cerro de Zonda. The section was measured in the NW corner of the Albarracín basin segment, ~8 km north of the section described by *Vergés et al*. [2001], in the footwall of the W dipping thrust fault responsible for the range referred to as the Cordón del Espinaco. The base of the SW dipping Albarracín section unconformably overlies the Devonian Punta Negra Formation and is offset by minor faults. Basin sedimentation occurred in close proximity to Miocene eruptive centers, including the Cerro Blanco 6 km to the east and Cerro la Sal 5 km to the north.

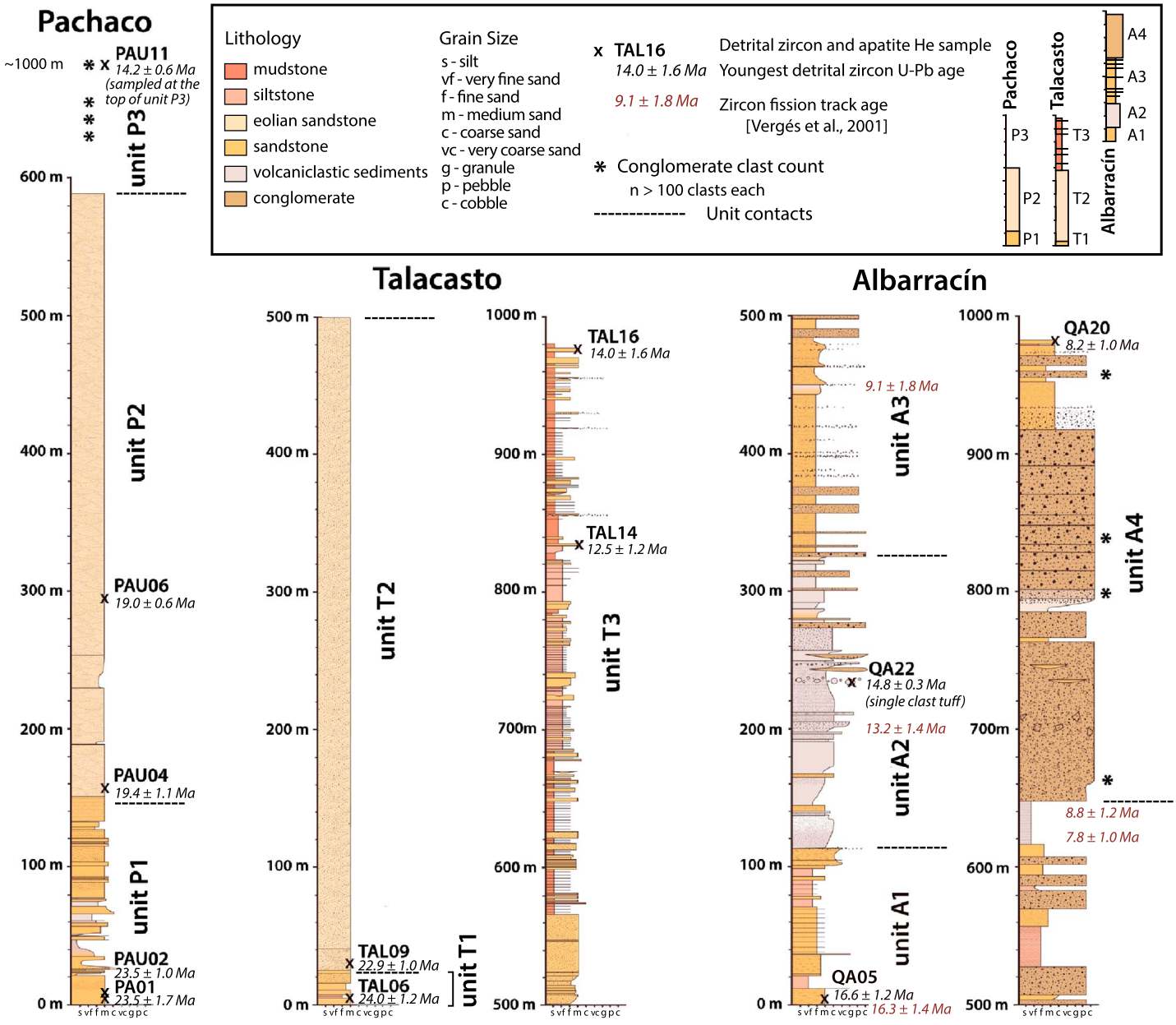

Figure 2. Measured stratigraphic sections of the Pachaco, Talacasto, and Albarracín localities showing the lithofacies distributions and the locations of conglomerate clast counts, detrital zircon and apatite (U-Th)/He samples, youngest detrital zircon U-Pb ages, and previous zircon fission track ages [from *Vergés et al.*, 2001].

3. Sedimentology

We measured three Cenozoic sections preserved in successive thrust sheets of the Precordillera, including clastic nonmarine fill of the 1000–1500 m Albarracín, ~1000 m Talacasto, and ~1000 m Pachaco successions (Figure 2). The uppermost Pachaco section was not measured directly but calculated from bedding orientations and internal stratigraphic contacts.

Sedimentary units were defined according to lithology, facies distribution, and inferred depositional processes (Figures 3–5 and Table 1; see Table S1 in the supporting information), then integrated into a depositional model with six main facies associations: mixed eolian-fluvial deposits (E1), eolian sandstones (E2), fine-grained distal fluvial/floodplain deposits (F1), tuffaceous volcaniclastic rocks (F2), medial fan braided channel sandstones (F3), and proximal fan conglomerates (F4). This model allows for spatial correlation among the measured sections and reconstruction of shifting depositional patterns.

Figure 3. Panoramic photographs of the Albarracín, Pachaco, and Talacasto sections. (a) View of the Albarracín section (560–700 m level) showing interbedded cross-stratified sandstones and conglomerates (unit A3, facies association F3) with a white ~16 m thick tuffaceous interval at the base of massive, pebble-cobble conglomerates (unit A4, facies association F4). (b) View of the Talacasto section with large-scale cross-stratified eolian sandstones (unit T2, facies association E2) overlain by reddish fine-grained floodplain deposits (unit T3, lithofacies F1). (c) View of the Pachaco section composed of pink to green, large-scale cross-stratified eolian sandstones (unit P2, lithofacies E2).

3.1. Phase A—Precursor Eolian System

3.1.1. Facies Association E1

Units P1 and TI of the lower Pachaco and Talacasto sections are characterized by medium to coarse-grained, moderately sorted, large-scale cross-bedded sandstones. Facies association E1 is distinguished from overlying eolian deposits (facies association E2) by its brighter color (maroon to bright green), sharp horizontal contacts, and nonreworked tuffaceous interbeds (Figures 4c and 4d). We attribute E1 deposits to mixed fluvial, eolian, and volcanic processes during a progressive transition to a regional eolian system. The ~1–10 m thick, cross-stratified sandstones have sharp flat basal surfaces, suggesting wetting of the eolian sediments during deflation of upper dune surfaces [*Langford and Chan*, 1989]. The distinctive color and presence of gypsum veins and cement may indicate long residence near the water table. Pachaco unit P1 deposits are ~100 m thicker and show more variation than unit T1 of the Talacasto section. Both successions include thin white pyroclastic ash beds, commonly with brown sandstone caps, and normally graded tuffaceous horizons deposited on top of deflated eolian surfaces. *Milana et al*. [1993] suggested deposition by infilling of swampy paleotopographic depressions and development of an ephemeral fluvial/playa lake regime, with progressive upsection drying and reworking during incipient development of eolian dune fields.

3.2. Phase B—Regional Eolian System

3.2.1. Facies Association E2

Units P2 and T2 of the Pachaco and Talacasto areas consist of ~400–500 m thick eolian deposits of facies association E2 (Figures 3b and 3c), though *Milana et al*. [1993] suggested a thickness up to 700 m. The sharp lower contacts of P2 and T2, marked by very large scale cross-stratified sandstone, represent an abrupt change to a fully developed eolian system. The deposits have ~2–10 m thick cross beds

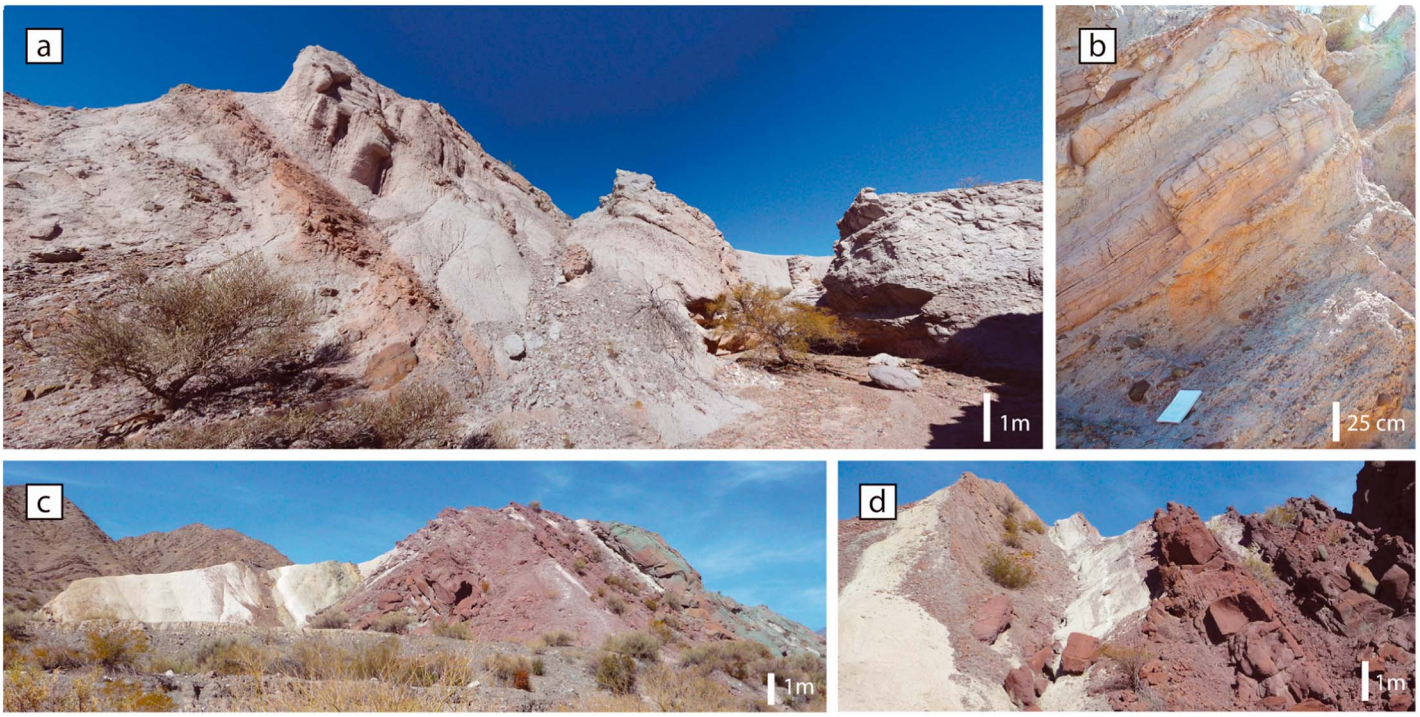

Figure 4. Field photographs of volcaniclastic intervals in the Albarracín and Pachaco sections. (a) Pyroclastic surge and ash flow deposits of the Albarracín section (unit A2, facies association F2). (b) Close-up photograph of tuffaceous deposits of unit A2 showing a very poorly sorted pyroclastic flow deposit with dispersed 1–2 cm pebbles of nonvolcanic Precordillera clasts at the base (lithofacies Ps) and finer-grained, thinly laminated ashfall tuff beds at the top. (c) Unit P1 (facies association E1) of the Pachaco section showing yellow to white tuffaceous intervals and thickly cross-stratified maroon and green sandstone beds. (d) A closer view of the interbedded sandstones (lithofacies Sd maroon beds) and volcaniclastic deposits (lithofacies Ps white beds) of unit P1.

(Figures 5c and 5d) with 1–25 cm thick foresets. Subhorizontal bounding surfaces are common, as are less consolidated, reworked tuffaceous intervals.

The fully developed E2 eolian system did not appear simultaneously. On the basis of the youngest detrital zircon U-Pb ages, eolian deposition commenced at 22.9 ± 1.0 Ma in the Talacasto area and 19.4 ± 1.1 Ma in the Pachaco area. Whereas the Talacasto section contains a thicker, light-colored tuffaceous interval at the base of eolian unit T2, most tuffaceous layers at Pachaco are thinly interbedded with P1 sandstones, possibly suggestive of a marginal dune field position with less volcanic input. *Milana* [1993] describes Oligo-Miocene eolian units ~150 km away in the Jáchal-Huaco area of the northern Precordillera, suggesting an extensive eolian system.

3.3. Phase C—Fluvial System (17–14 Ma)

3.3.1. Facies Associations F1 and F3

In the Talacasto area, eolian deposits are sharply capped by fluvial deposits of unit T3, including a 1 m mudstone and a 66 m interval of medium- to coarse-grained, cross-bedded sandstone and thin, dark red mudstone interbeds. The sandstones form stacked channels, some with coarse granular lags. Upper T3 consists of finer overbank fluvial deposits (facies association F1; Figure 5a): poorly lithified, thinly interbedded, poorly sorted red claystone, siltstone, and sandstone with small-scale cross lamination (lithofacies Fl). Interbedded sandstones include isolated channel deposits (lithofacies Sr, Sh, and Ss), cross-bedded sandstones (lithofacies St) with pebbly erosional bases and/or mud rip-up clasts representing channel scours [*Guion*, 1984], and tabular, parallel-laminated sandstones representing distal crevasse splay deposits.

In the Albarracín area, basal unit A1 (112 m thick) has a higher proportion of thinly bedded, very fine grained sandstones but is otherwise similar to the T3 deposits of the upper Talacasto succession (Figures 5a and 5b). We interpret A1 to represent deposition in distal fluvial floodplains, consistent with the roughly equivalent depositional ages for the upper Talacasto and lower Albarracín sections (Figure 2).

In the Pachaco area, fluvial unit P3 is much coarser grained than underlying eolian deposits and characterized by gravelly, cross-bedded sandstones and conglomerates of facies association F3. The sandstones (lithofacies St) are

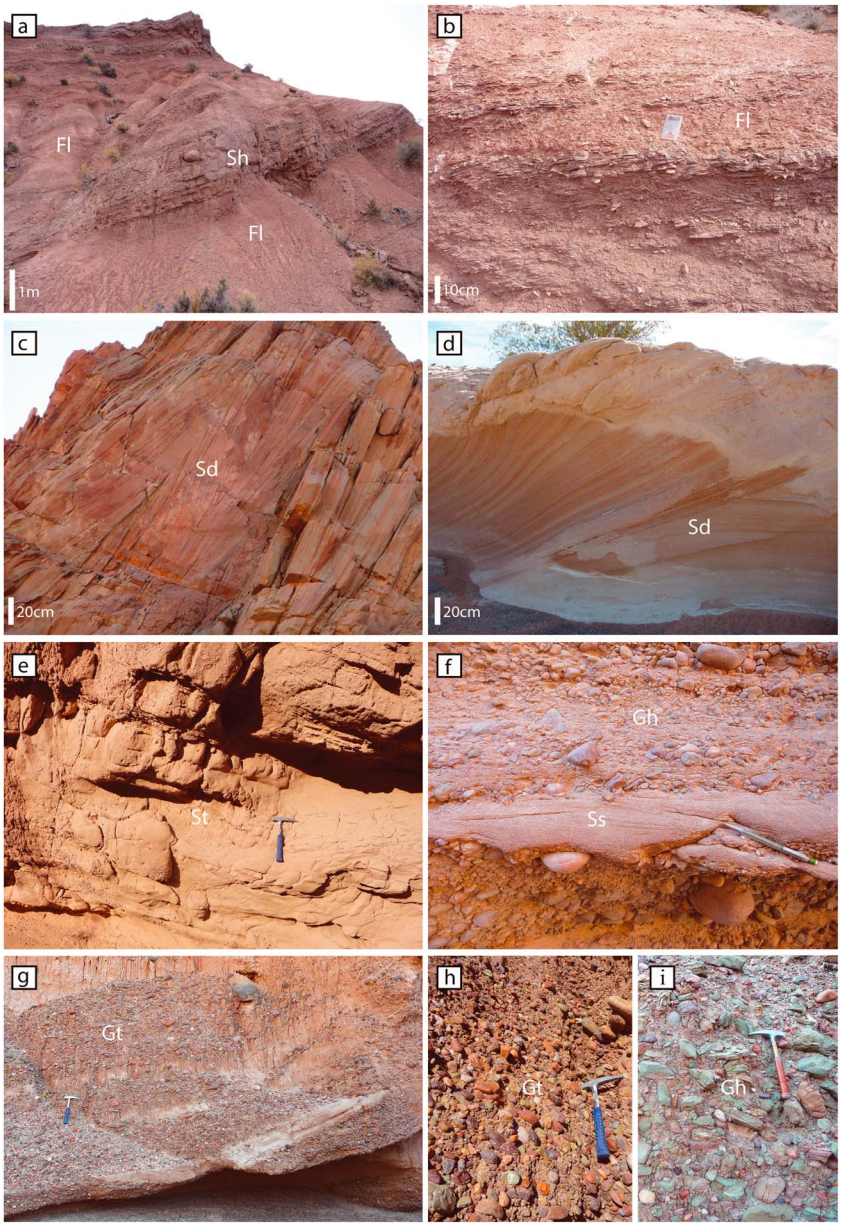

Figure 5. Field photographs of sedimentary deposits of the Pachaco, Talacasto, and Albarracín sections. (a) Reddish, poorly consolidated, finely laminated claystone to siltstone with very thin, very fine to fine sandstones (lithofacies Fl) and a ~1 m thick, planar-laminated sandstone bed of lithofacies Sh at Talacasto (unit T3). (b) Close-up of lithofacies Fl of Albarracín unit A1. (c, d) Large-scale cross-stratified eolian sandstone (lithofacies Sd) at Pachaco (unit P2) and Talacasto (unit T2). Interbedded cross-stratified sandstones and conglomerates of facies association F3 at Albarracín (unit A3): (e) tan, trough cross-bedded sandstone (lithofacies St); (f) tan, coarse-grained scour-fill sandstone (lithofacies Ss), overlain by horizontally bedded pebble conglomerate (lithofacies Gh), and (g) laterally discontinuous, poorly sorted, clast-supported pebble conglomerate with medium to coarse sandstone matrix and discontinuous lenses of sandstone (lithofacies Gt). (h) Close-up of a clast-supported pebble conglomerate (lithofacies Gt) at Albarracín (Unit A4), showing a mix of igneous Choiyoi and nonigneous Precordillera clasts. (i) Close-up of a clast-supported breccia (lithofacies Gh) at Albarracín (Unit A4), compositionally dominated by green to pink sandstone Precordillera clasts.

medium-grained, trough cross-stratified beds with granule or pebble lags. Laterally, they interfinger with pebble conglomerates (lithofacies Gt). The coarser grain size, trough cross stratification, erosive bases, and lenticular bed geometries of the upward coarsening P3 unit represent a proximal gravel-sand braided fluvial system [*Miall*, 1996]. The proximity of Pachaco to the orogenic front explains the coarser nature of the P3 unit relative to age equivalent strata of upper Talacasto T3 unit and lower Albarracín A1 unit.

Table 1. Summary of Facies Associations and Interpretations

Facies Association	Lithofacies	Description	Stratigraphic Occurrence	Interpretation
E1. Dune cross-stratified sandstone with fine tuffaceous interbeds	Sd, Pm, Sme	Brightly colored maroon to bright green dune cross-bedded sandstones with sharp, flat bedding contacts and thin, very fine, white tuffaceous interbeds	Units P1 and T1	Fluvial-eolian deposits (wet eolian system)
E2. Large-scale cross-stratified eolian sandstone	Sd	Tan pinkish to greenish, thick sandstone deposits with large-scale cross stratification	Units P2 and T2	Eolian dune field deposits (dry eolian system)
F1. Finely interbedded mudstones, siltstones, and sandstones	Fl, Sr, Sh, Ss	Reddish orange, finely laminated, thinly interbedded clays, silts, and sands; thicker sandstone intervals are either cross bedded, with erosional bases and pebbly lags and mud rip-up clasts or parallel laminated and no thicker than 50 cm	Units T3 and A1	Overbank sedimentation in an alluvial plain setting with occasional crevasse splay deposits
F2. Pyroclastic surge and epiclastic sandstones and conglomerates	Pm, Sme, She, Gme	White to gray tuffaceous beds with coarser massive to horizontally bedded pebbly intervals with various degrees of sorting; fluvially reworked epiclastic sandstones interbeds and pebble conglomerate lenses common toward the top of the section	Unit A2	Pyroclastic surge and fall deposits
F3. Interbedded cross-stratified sandstones and conglomerates	St, Gt, Ss	Fine to course, through cross-bedded sandstones with pebble lags and common erosive bases; pebble lens and sandy pebble conglomerate beds interfinger with the sandier intervals	Units P3 and A3	Gravel-sand braided stream deposits in middle alluvial fan setting
F4. Massive, cross-bedded, and horizontally bedded sandy matrix conglomerates	Gme, Gt, Gh, St	Pebble to cobble clast and matrix-supported conglomerates with a sandy matrix and pebbly sandstone lenses; some beds save subtle horizontal stratification and sorting. Whiter intervals have a significant tuffaceous component in the matrix and support a dispursed mixture of clasts of varying sizes and angularities	Unit A4	Gravel distributary fluvial and debris flow deposits in a proximal fan setting

3.4. Phase D—Volcaniclastic System

3.4.1. Facies Association F2

Unit A2 of the Albarracín section overlies distal fluvial deposits and consists of a >200 m interval of grayish-white volcaniclastic deposits from nearby igneous centers (Figures 4a and 4b), including pyroclastic surge and ash flow deposits (lithofacies Ps), ashfall deposits (lithofacies Pm), and fluvially reworked epiclastic intervals with nonpyroclastic sandy and pebbly detritus (lithofacies Sme and Gme). The pyroclastic flows are thick bedded and very poorly sorted, with andesite, nonpyroclastic green sandstone, and pebbles and granules of Precordillera lithologies distributed throughout. Some crudely bedded intervals include Precordillera clasts up to 80 cm in diameter. Finer-grained deposits with better sorting and planar lamination are interpreted as ash-cloud surge deposits [*Bercowski and Figueroa*, 1987; *Vergés et al*., 2001]. In upper A2, gravel channel lenses and tabular pebbly sandstones become increasingly common as the volcaniclastic system transitioned to a fluvial environment.

3.5. Phase E—Progradation of Fluvial System

3.5.1. Facies Associations F3 and F4

Units A3 and A4, the youngest deposits studied, are exposed in the Albarracín area above volcaniclastic unit A2 and record the progradation of fluvial systems. These deposits correspond to the previously described upper Albarracín Formation [*Leveratto*, 1968] and units III and IV [*Vergés et al*., 2001] and attain a thickness of ~660 m. The sandier unit A3 is lithologically similar to the upper Pachaco unit P3 (facies association F3) but contains volcaniclastic intervals toward the top (Figure 3a).

Conglomeratic unit A4 records proximal deposition of alluvial fan facies. It is composed of subangular to subrounded sandy conglomerates showing crude cross stratification with medium- to coarse-grained pebbly sandstone lenses (lithofacies Gt), cobble conglomerates with subtle horizontal bedding (lithofacies Gh),

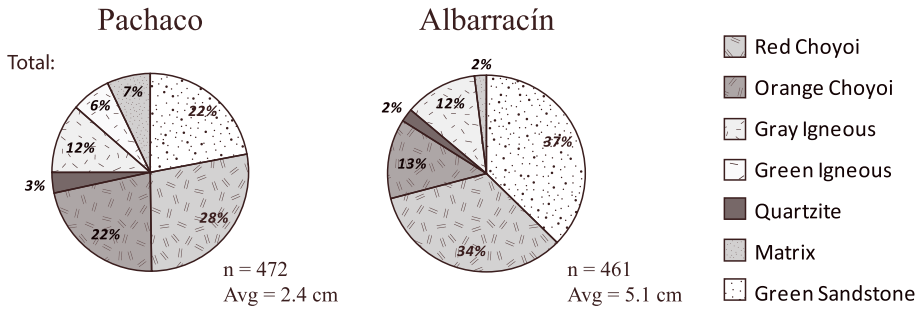

Figure 6. Pie charts showing conglomerate clast count results at Pachaco (unit P3 of the Pachaco section and unit A4 of the Albarracín section, combined from four stations at each locality (Figure 1)). The total number of clasts and the mean clast diameter are reported next to each pie chart.

andmatrix-supported pebble-cobble conglomerates with large angular clasts and significant tuffaceous matrix (lithofacies Gme). These deposits are indicative of gravelly stream flows, sheet flows, and debris flows of an alluvial fan setting.

4. Sediment Provenance

Basin sediments are derived from western sources—dominantly the Frontal Cordillera, with partial input from the westernmost Precordillera. Paleocurrent measurements for the Albarracín section [*Vergés et al*., 2001] show consistent eastward transport with limited dispersion. Southward paleocurrents within Albarracín pyroclastic deposits are indicative of local paleoslopes related to nearby eruptive centers [*Vergés et al*., 2001]. Regionally, eastward paleoflow is apparent from lateral facies variations. Initial deposits recorded sandy-gravelly braided stream sedimentation while regions farther east recorded distal floodplain deposition of thin-bedded mudstone and sandstone. Eastward propagation of the deformation front introduced detritus from Precordillera thrust sheets to basin areas, a pattern correlated with a grain size increase best expressed in the Albarracín section, where cross-stratified sandstone is capped by thick, pebble-cobble alluvial fan conglomerate. Conglomerate clasts originated from both the Frontal Cordillera and Precordillera, with minor proportions of Cenozoic volcanic clasts. For the upper Albarracín section, *Vergés et al*. [2001] reported an increase in Precordillera clasts from 10% in unit A3 to 70% at the base of unit A4, dropping to 40% at the top of the section —a pattern suggestive of enhanced exhumation in the Precordillera.

4.1. Methods

We collected conglomerate clast size and composition data (Figures 6 and S3) at eight sites throughout the upper Pachaco (unit P3) and upper Albarracín sections (unit A4). At each site, we measured over 100 clasts at ~10 cm grid intersections in a 1 m^2 area [*Howard*, 1993]. Clasts were binned by color and lithology, with most Frontal Cordilleran versus Precordilleran clasts readily distinguished (Figures 5h and 5i). Frontal Cordillera clasts are gray, orange, and pink to maroon rhyolites, andesites, and dacites of the Choiyoi Group and are typically rounded to subrounded. Precordillera clasts consist of dark green and subordinate maroon, well-lithified, fine to medium sandstones from Silurian-Devonian units. A minor population consists of vein quartz pebbles and green igneous pebbles, likely originating from the Frontal Cordillera.

4.2. Results

At Pachaco, clast compositions are dominated by a variety of Frontal Cordillera clasts, with a steady 20–30% proportion of Precordillera clasts throughout unit P3. At Albarracín, the proportion of Precordillera clasts averages 37% and reaches 55% at the base of conglomeratic unit A4 (*Vergés et al*. [2001] report up to 73%). The upsection increase in Precordillera detritus and increase in mean clast size from 2.4 cm at Pachaco to 5.1 cm at Albarracín are considered indicative of increasing Precordillera deformation during basin filling. Within the Albarracín section, however, a decrease in Precordillera clasts is expressed within unit A4. This trend also appears in compositional data reported by *Vergés et al*. [2001] in the upper 300 m of their measured Albarracín section; they attribute increased Frontal Cordillera clasts to recycling of older Cenozoic sediments by Precordillera thrusting.

Interestingly, increases in Frontal Cordillera clasts in upper clast counts correlate with smaller clast size and a higher proportion of sandy facies. Clast counts yielding only 20–30% Precordillera clasts characterize thinner conglomerate beds in sandstone-dominated fluvial intervals of facies association F3 (gravel-sand braided deposits). The reduction in Precordillera clasts may be explained by sediment routing systems in which finer distal materials interacted with more proximal systems responsible for massive conglomerates in unit A4. The shift to sandier facies at the top of the Albarracín section may represent lateral shifts in a distal fluvial system from the Frontal Cordillera versus proximal alluvial fans from adjacent Precordillera structures. Alternatively, the shift could be indicative of (1) a pause in local tectonic activity in the axial to eastern Precordillera around 8 Ma, with a corresponding reduction in sediment delivery from this zone, (2) increased uplift and sediment delivery from the Frontal Cordillera, and/or (3) large-scale reorganization of sediment routing systems.

5. Detrital Zircon U-Pb Geochronology

U-Pb analyses of 12 basin fill samples were employed to determine sediment provenance and to constrain depositional ages in order to establish more precise sedimentation histories and chronostratigraphic correlations among the sections.

5.1. Methods

We collected samples throughout the Pachaco, Talacasto, and Albarracín successions and processed 11 medium-grained sandstones and a single clast tuff according to standard heavy liquid separation techniques. The nonmagnetic heavy mineral fraction was poured onto a tape mount and analyzed by laser ablation ICP-MS (inductively coupled plasma mass spectrometry) at the University of Texas at Austin. Samples were loaded into a large-volume Helex sample cell and analyzed with a magnetic sector, single-collector Element2 high-resolution ICP-MS inductively coupled plasma mass spectrometry with an Excimer laser ablation system.

For each sample, over 130 zircon grains were selected, with the exception of one sample (PAU06) with limited zircon. Grains were chosen at random and varied in size, shape, and quality. The 30 μm laser ablation spot was placed carefully to avoid cracks, inclusions, and grain edges. GJ-1 zircon (600.4 ± 0.1 Ma) was used as a reference standard. Data were reduced with Iolite software (www.iolite.org.au; Table S2). Since a tape mount rather than a polished mount was employed, initial laser ablation resulted in a depth profile of the outermost ~16 μm layer of individual grains. A small fraction of grains showed distinct core and rim ages, for which both ages were used in further data analysis. U-Pb results are summarized and plotted as age histograms and relative probability distribution curves (Figures 7 and 8).

5.2. Results

5.2.1. Depositional Ages

Each sample contained abundant Cenozoic grains associated with Andean arc magmatism. On average, over 50% of analyzed zircons were younger than 45 Ma; in one sample, as many as 113 grains (>90%) were younger than 35 Ma. Although recycled sediment dominates over primary volcanic materials in most Andean basins [*Jordan*, 1995], the tuffaceous component of many stratigraphic levels and proximity to igneous centers [*Kay and Mpodozis*, 2002; *Vergés et al*., 2001] help explain the strong volcanic contribution. For several reasons, we interpret the youngest zircon age in each sample to be very close to the depositional age of the host rock. First, a systematic upsection decrease is expressed in both the mean ages and youngest grain ages for all three sections (Figure 7). Second, within each sample, the youngest grain ages consistently represent the youngest portion of a broader Cenozoic population. Third, each sample displays a tight cluster of ages, with the second-youngest grain consistently within 2σ error of the youngest grain age (Figure 9).

All three measured sections represent roughly 10 Myr, ranging from latest Oligocene to late Miocene time. At Pachaco, the two lowest samples yield 23.5 ± 1.7 Ma youngest zircon ages, two samples from the middle eolian unit are ~19 Ma, and the upper sample is 14.2 ± 0.6 Ma. The Talacasto section 50 km to the NE has comparable upper and lower age bounds: 24.0 ± 1.2 Ma and 14.0 ± 1.6 Ma, respectively. However, the base of the Talacasto eolian unit contains youngest zircons of 22.9 ± 1.0 Ma, slightly older than the ~19 Ma eolian unit at Pachaco. At Albarracín, the basal sample records an age of 16.6 ± 1.2 Ma, coeval with the Cerro la Sal eruptive center ~4 km north of the section and in good agreement with the 16.3 ± 1.4 Ma zircon

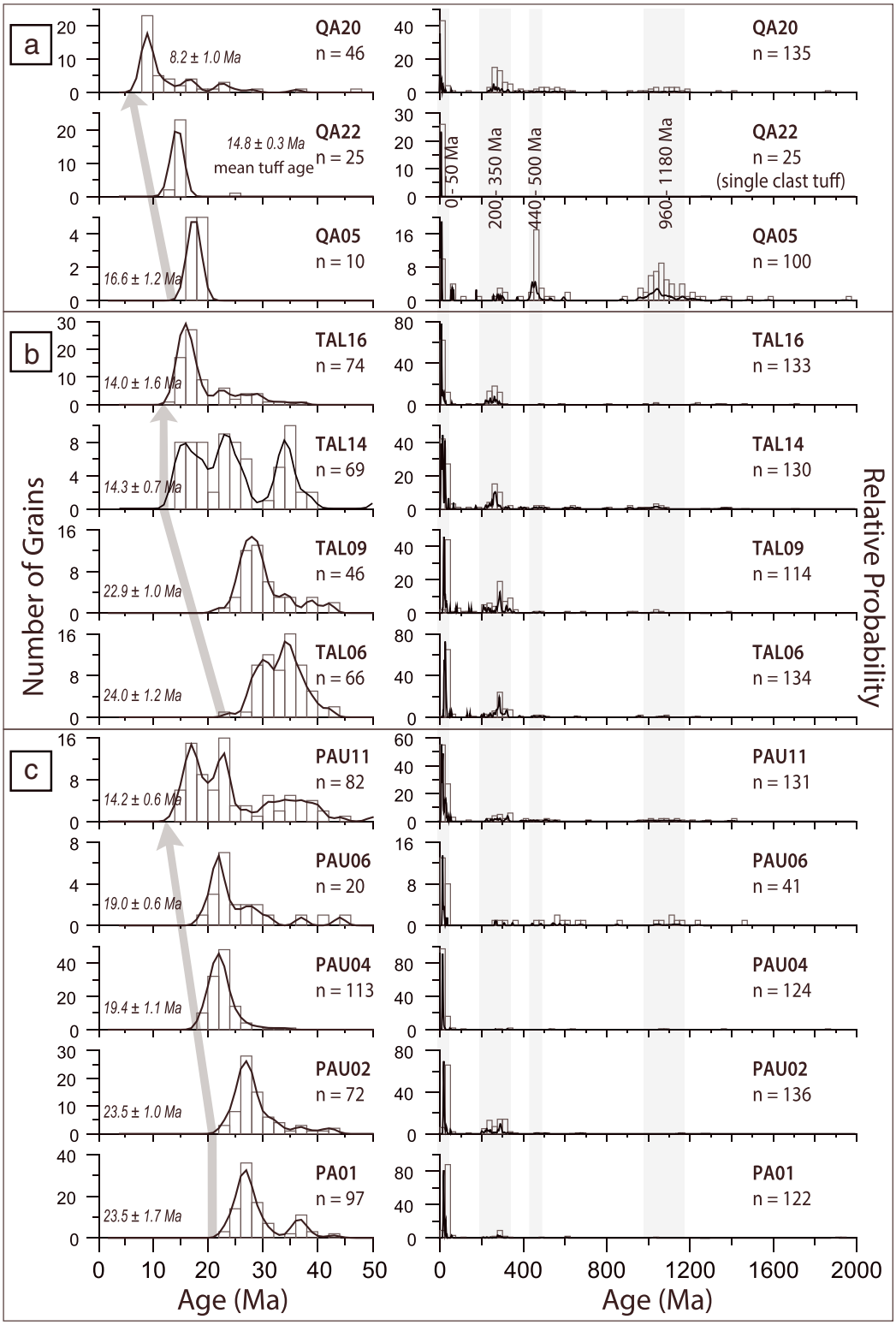

Figure 7. Detrital zircon U-Pb data plotted as relative age probability curves (thick smooth lines) and age histograms (thin rectangles) for (a) Albarracín, (b) Talacasto, and (c) Pachaco samples. U-Pb ages for each sample are depicted in two plots. Plots on the left (0–50 Ma) emphasize the contribution of Cenozoic zircon grains; plots on the right (0–2000 Ma) show the overall distribution of detrital zircon ages. Samples are arranged by locality in stratigraphic order, from older levels (base) to younger levels (top), with the youngest single detrital zircon age reported for each sample. Shaded arrows indicate progressive upsection younging of Cenozoic age populations in all three sections (Pachaco, Talacasto, and Albarracín).

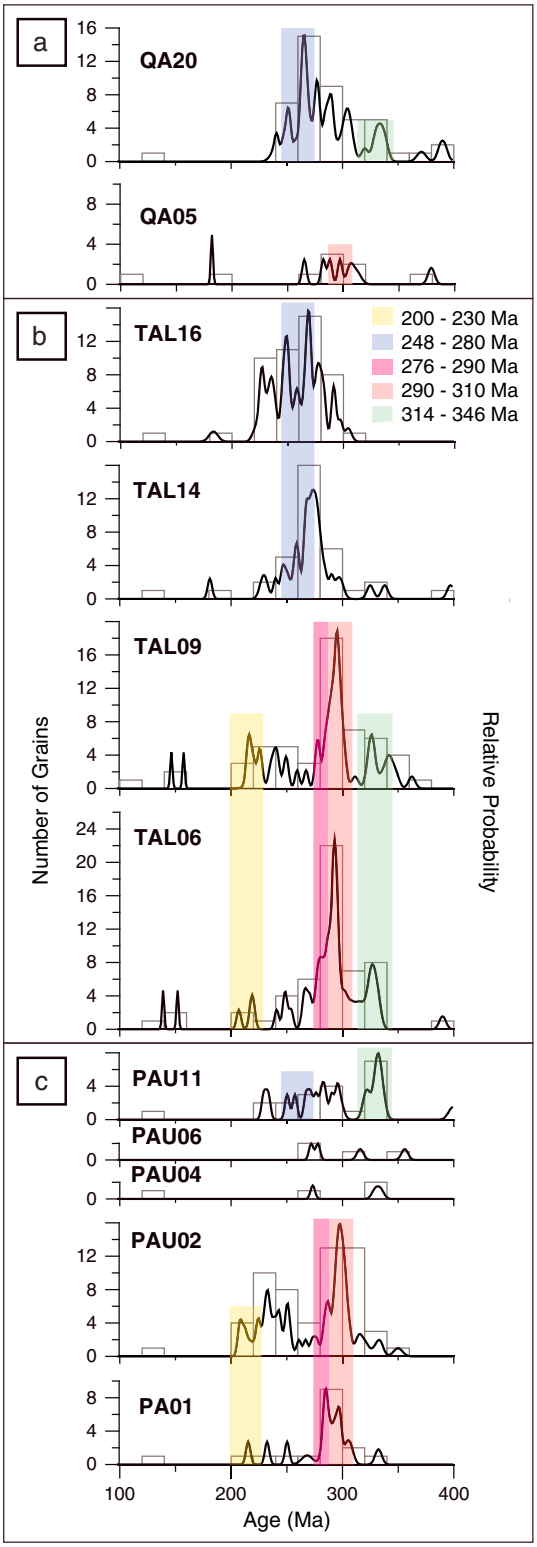

fission track age reported by *Vergés et al*. [2001]. The 8.2 ± 1.0 Ma youngest zircons in the upper Albarracín sample were also locally derived, likely from the Cerro Blanco igneous center to the east. This late Miocene age agrees with the 8.8 ± 1.2 Ma and 7.8 ± 1.0 Ma fission track ages reported for the base of the conglomeratic unit [*Vergés et al*., 2001], but the similarity (overlap in errors) of these ages for the base and top of the 350–400 m thick conglomeratic unit implies very rapid accumulation. In addition to sandstone samples near the base and top, we also analyzed 25 zircon grains from a single clast of andesitic tuff, situated 235 m above the basal sandstone sample, which yield an average age of 14.8 ± 0.3 Ma. The middle Miocene age for this unit is slightly older but within error of the 13.2 ± 1.4 Ma age reported by *Vergés et al*. [2001], possibly due to lateral variations in igneous source or incorporation of older tuffaceous material.

5.2.2. Provenance

The analyzed samples record up to four major zircon U-Pb age populations: (1) Cenozoic, (2) early Mesozoic to late Paleozoic, (3) early Paleozoic, and (4) Mesoproterozoic.

1. Cenozoic age peaks range from 45 to 8 Ma, with most zircons ($n = 385$) between 30 and 20 Ma, the beginning of the modern Andean magmatic cycle and a period of rapid Nazca-South America convergence [*Pardo-Casas and Molnar*, 1987; *Kay et al*., 1988; *Kay and Abbruzzi*, 1996]. The ages are attributed to an influx of first-cycle volcanic zircons related to arc magmatism [*Kay and Mpodozis*, 2002].
2. The second prominent cluster of ages ranges between 365 and 208 Ma, with a major Permo-Triassic signal related to widespread Choiyoi Group magmatism in an extensional or transtensional setting [*Giambiagi and Martinez*, 2008; *Ramos*, 2009; *Ramos and Kay*, 1991; *Ramos*, 1995]. The lowest samples in each section are characterized by a strong age peak around 297 Ma and shoulder sloping toward 276 Ma

Figure 8. Detrital zircon U-Pb data plotted as relative age probability curves (thick smooth lines) and age histograms (thin rectangles) for (a) Albarracín, (b) Talacasto, and (c) Pachaco samples. Samples are arranged by locality in stratigraphic order, from older levels (base) to younger levels (top). Note the similarities in U-Pb age distributions for eolian sandstone samples from lowermost stratigraphic levels (PAU02 and TAL09; Figure 2) and for fluvial sandstone samples from upper stratigraphic levels (TAL14, TAL16, and QA20; Figure 2). Color-shaded rectangles identify different detrital zircon populations (see text for discussion).

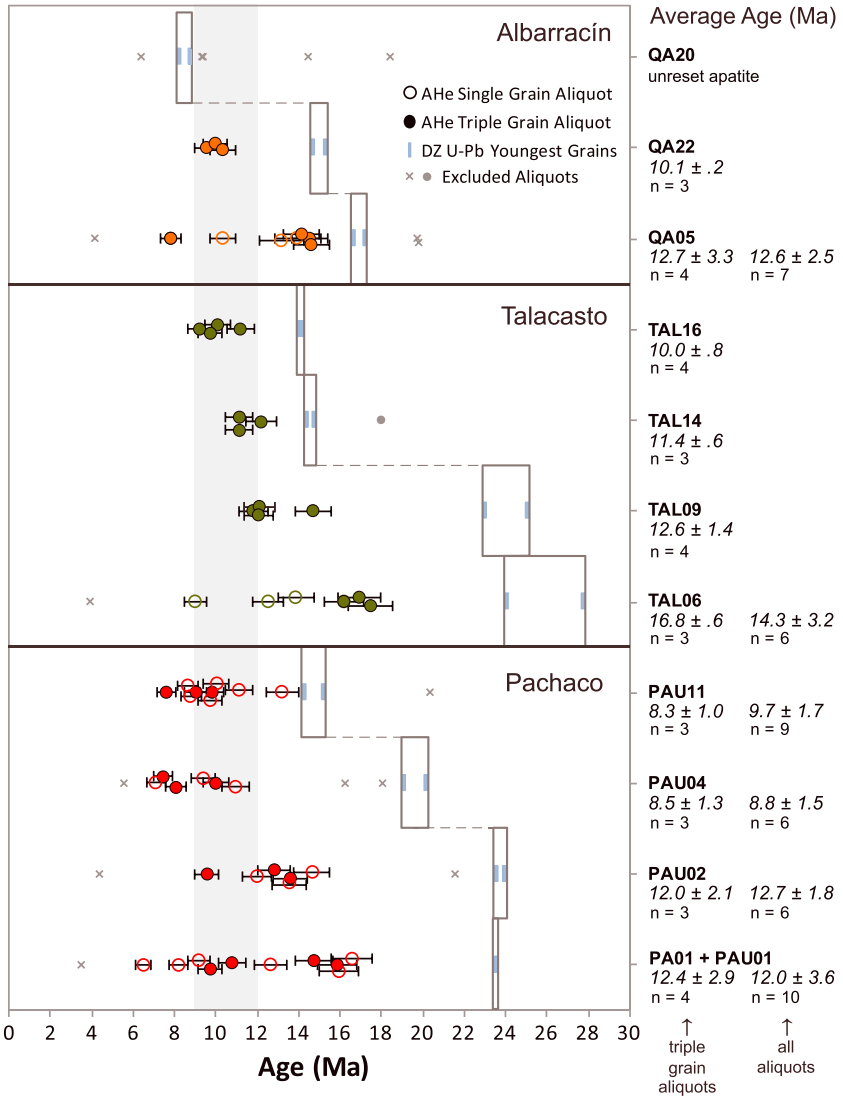

Figure 9. Plot of apatite (U-Th)/He ages for the Albarracín, Pachaco, and Talacasto sections from single-grain aliquots (open circles) and triple-grain aliquots (closed circles). All (U-Th)/He ages are plotted with 2σ error bars. For each locality, samples are presented in stratigraphic order, with maximum depositional ages denoted by tall gray boxes where the two youngest U-Pb ages (short blue bars) define the box edges. With the exception of the highest Albarracín sample (QA20), the apatite (U-Th)/He ages are systematically younger than their corresponding U-Pb ages, indicating that apatites were thermally reset after deposition by later burial reheating. Small gray crosses and one gray solid circle denote, respectively, single-grain ages and a triple-grain aliquot age excluded from age calculations. The gray bar shading for the 12–9 Ma region represents the period of rapid exhumation in the Precordillera.

(Figures 7 and 8). We interpret this Early Permian signal to be a first-cycle zircon population from the Lower Choiyoi Group (276–290 Ma), with possible recycling from the Upper Carboniferous-Permian Agua Negra Formation [*Aparicio*, 1969; *Polanski*, 1970]. In contrast, younger samples have prominent peaks from 280 to 248 Ma and diminished older Choiyoi peaks, suggesting a stronger contribution from post Lower Choiyoi units. *Rocha-Campos et al.* [2011] report U-Pb ages for the Middle and Upper Choiyoi sections of 265 Ma and 252 Ma, respectively. The overall Permo-Triassic signal could be further enhanced by contributions from granitic rocks of this age in the Frontal Cordillera.

Late Triassic zircons (230–200 Ma) originate from granitic plutons in the Frontal Cordillera or recycled basin fill (such as the Rincon Blanco Group) of the Triassic Cuyo rift south and west of the Precordillera [*López-Gamundí and Astini*, 2004]. Although Triassic zircons appear in the Talacasto and Pachaco sections,

they are absent from Albarracín samples (Figure 8), possibly suggesting drainage reorganization due to tectonic activity in the Frontal Cordillera or initial Precordillera thrusting.

A Carboniferous peak (346–314 Ma) appears in the two lower Talacasto samples but is present only in the uppermost Pachaco and Albarracín samples. Granites in the Sierras Pampeanas to the east yield U-Pb ages in the 360–330 Ma range [*Grosse et al.*, 2009]. It is plausible that zircons derived from such granites were deposited and later recycled from Carboniferous-Triassic rocks exposed in the Frontal Cordillera (in the case of the lower Talacasto samples) or Precordillera (in the case of the upper Pachaco and Albarracín samples).

3. Age clusters around 500–440 Ma and 1180–960 Ma are minor in comparison to the Cenozoic and Paleozoic age populations and are present only in uppermost Pachaco and Albarracín samples (Figure 7). Ordovician zircons in the 490–460 Ma range are derived from the Famatinian magmatic arc east of the Precordillera [*Dahlquist et al.*, 2008; *Pankhurst et al.*, 2000], whereas late Mesoproterozoic-early Neoproterozoic zircons (1200–900 Ma) likely originate from various cratonic blocks [*Ramos*, 2009]. Both detrital zircon signatures are represented in Paleozoic rocks of the Precordillera [*Finney et al.*, 2005]. For the basal Albarracín sample (QA05), the prominence of these age populations suggest local exposure of the Paleozoic bedrock surface (including the underlying Devonian Punta Negra Formation) prior to organized large-scale Cenozoic subsidence. However, for samples from uppermost basin fill (PAU11 and QA20), the presence but limited quantity of these zircons suggests that some Precordillera rocks had been regionally thrust up to the surface by the time of late Miocene deposition.

6. Apatite Helium Thermochronology

(U-Th)/He thermochronometry measures radiogenic He daughter relative to parent isotopes (U, Th, and Sm) retained within a mineral grain, most commonly apatite or zircon. He is produced as alpha particles during radioactive decay of ^{238}U, ^{235}U, ^{232}Th, and ^{147}Sm. He is retained after the mineral cools below a certain threshold or closure temperature, recording either a post crystallization cooling age of host rock or the timing of exhumational cooling of a rock that was previously reheated (i.e., a reset apatite helium age). The apatite (U-Th)/He system (AHe) has a closure temperature of ~50–110°C, depending on radiation damage and other factors [*Flowers et al.*, 2009; *Shuster et al.*, 2006], and is widely applicable to upper crustal processes [*Ehlers and Farley*, 2003; *Rahl et al.*, 2007]. We use AHe thermochronometry to study the cooling history of three basin segments and constrain the timing of uplift-induced exhumation in the Precordillera.

AHe thermochronometry requires careful grain selection and data analysis because AHe ages can be influenced by factors that affect the amount of He and its parent isotopes. He retentivity within individual apatites depends on temperature as well as radiation damage and grain size (due to He diffusional loss at grain edges) [*Ehlers and Farley*, 2003; *Farley and Stockli*, 2002; *Shuster et al.*, 2006]. Heavy radiation damage due to high concentrations of U, Th, and Sm parent isotopes (known as [eU], the effective uranium concentration) alters the diffusion kinetics of He and therefore the age of a grain [*Flowers et al.*, 2009]. Zonations of parent isotope concentrations, variations in apatite chemistry, and the presence of inclusions or other imperfections within a grain may also lead to higher uncertainty for the corresponding AHe ages [*Farley*, 2000, 2002; *Reiners and Farley*, 2001]. Because these factors affect individual grains, the reproducibility of AHe ages from multiple aliquots for each sample is a good measure of the validity of a sample's age.

6.1. Methods

Mineral separations were comparable for both apatites and zircons. Samples first went through crushing, water table, heavy liquids (Bromoform), and Frantz magnetic separation. Apatites were then picked under a microscope from the heavy nonmagnetic fraction, and some remaining grains were poured onto tape mounts for U-Pb analyses. Consequently, the apatite helium results and zircon U-Pb results may be compared consistently for each sample.

Because nearly all samples are detrital, six to eight apatite grains were carefully chosen from each sample to ensure reproducibility, and two aliquots of Durango apatite were analyzed along with each batch of samples as an internal laboratory standard. Only high-quality apatites free of cracks and inclusions were selected.

When possible, we chose euhedral grains 70–150 μm in diameter; however, in poorer samples, clear and inclusion-free grains >60 μm and slightly abraded or chipped grains were also selected. The apatites were photographed and measured, and a standard F_T correction was applied to each grain to account for He loss in the outer 20 μm of the grain, following methods of *Farley et al*. [1996], *Farley and Stockli* [2002], and *Ehlers and Farley* [2003]. Grains were then sealed into separate platinum foil packets to be loaded into the ^{4}He extraction line. Samples were heated to ~990°C by a diode laser for 5 min and the released gas spiked with ^{3}He was analyzed by a quadrupole mass spectrometer to determine the [^{4}He] of each apatite grain. Samples were then dissolved with a HNO_3-based solution containing a ^{235}U, ^{230}Th, and ^{149}Sm tracer and subsequently diluted with 500 μL of ultrapure H_2O and allowed to equilibrate at room temperature for 24 h. The dissolved aliquots were analyzed using a Thermo Element2 inductively coupled plasma mass spectrometry to determine the ^{238}U, ^{235}U, ^{232}Th, and ^{147}Sm concentrations. The reported AHe ages are quoted with a 6% (2σ) analytical uncertainty calculated with respect to the reproducibility of laboratory standards. An average age for each sample is reported as an arithmetic mean with a standard deviation calculated from the aliquot ages.

Apatites in these samples contain anomalously low He (<0.1 nmol/g) and U (<1 ppm), which introduces a higher uncertainty in calculated ages because the measured elemental concentrations are close to instrumental blank values. To reduce this uncertainty and improve reproducibility, it is common to use multigrain aliquots to boost the signal of He and U [*Persano et al*., 2007; *Vermeesch*, 2008]. Therefore, we picked an additional nine to 12 apatites from each sample, depending on the availability of suitable grains, and sealed three apatite grains into each Pt foil packet, resulting in three to four multigrain aliquots per sample. The analytical procedures were identical to the single-grain analyses, except that the mass-weighted mean of individual grain F_T values was used for the F_T correction of each aliquot [*Farley and Stockli*, 2002].

6.2. Results

We analyzed apatite grains from 11 sandstone samples and a single clast of tuff from Neogene basin fill—the same samples analyzed for U-Pb geochronology, with the exception of TAL06, which did not contain high-quality apatite. The results (Figure 9 and Table S3) show no correlation between apatite (U-Th)/He (or AHe) age and grain size, morphology, or [eU]. Analyzed apatites were exceptionally low in effective uranium: most single-grain aliquots had <2 ppm [eU] and triple-grain aliquots had <10 ppm [eU] (Figure S2a). Because of these low He and U concentrations, the single-grain AHe data show broad age spreads; the triple-grain aliquot AHe data fall in the range of the single-grain data and show better reproducibility. Out of 35 triple-grain aliquots, only two were omitted: one due to instrumental error and another due to an erroneous age likely resulting from a high U or Th inclusion.

From the ~1000 m Pachaco section, we collected six medium sandstone samples: three from lower stratigraphic levels, two in the middle eolian unit (one of which yielded no apatites), and one at the top. All samples were collected at 1500–1600 m elevation. The basal samples (PA01, PAU01, and PAU02) are essentially stratigraphic equivalents and yield very similar AHe ages that cluster around 12 Ma, with a combined average age of 12.2 ± 3.0 Ma. The middle and upper samples have slightly younger and more tightly clustered AHe ages, averaging between 8.3 and 9.7 Ma. All AHe ages from the five analyzed Pachaco samples are significantly younger than their corresponding youngest detrital zircon U-Pb ages; therefore, we assume that the AHe ages have been reset and may be interpreted as cooling ages of Pachaco basin fill.

At Talacasto, four samples were analyzed: two near the base and two near the top of the 1000 m section, collected at 1550–1635 m elevation. AHe ages for the Talacasto samples show a similar upsection younging trend. The lowest sample shows a moderate spread in AHe ages, with single-grain aliquots averaging 11.8 ± 2.5 Ma and triple-grain aliquots averaging 16.8 ± 0.6 Ma. Approximately 100 m above this sample, three of the four aliquots from TAL09 average 11.9 ± 0.2 Ma, and the two highest samples have similar ages of 11.4 ± 0.6 Ma (TAL14) and 10.0 ± 0.8 Ma (TAL16). Despite several anomalously old AHe ages at the base of the section, the majority of Talacasto AHe ages fall between 12 and 10 Ma.

Finally, in the Albarracín section we have data from two sandstones at the base and top of the 1000 m section and a single clast of tuff collected ~230 m above the base. Samples were collected at 1040–1180 m elevation. The basal sandstone has a mean AHe age of 12.6 ± 2.5 Ma. The single tuff clast has a very reproducible age of 10.1 ± 0.2 Ma based on three aliquots of clear, inclusion-free volcanic apatite, underscoring the effect of high-quality grains on reproducibility of AHe data. This tuff clast has a U-Pb age of 14.8 ± 0.3 Ma, indicating

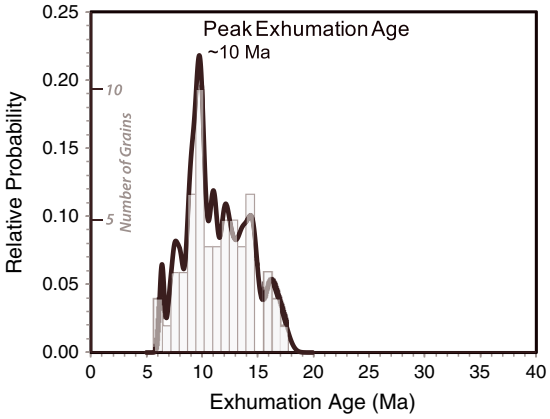

Figure 10. Probability density plot and histogram of all apatite (U-Th)/He ages ($n = 59$) from Pachaco, Talacasto, and Albarracín samples (summarized in Figure 9). Ages between 12 and 9 Ma make up the highest probability peak, with a mean around 10 Ma, interpreted to be the peak exhumation age in the Precordillera.

that AHe ages from the lower half of the Albarracín section have been reset. The highest sample has an age signature that has not been reset by post depositional burial heating. The AHe ages range from 18.4 to 6.3 Ma, whereas the youngest zircon from this sample is 8.2 ± 1.0 Ma, indicating that apatites have not been buried to sufficient depths for thermal resetting. This is not surprising given that this sample is from the highest levels of all three sections. Nevertheless, the amount of overlying basin fill or thrust sheet overburden remains unclear. A nonreset conglomeratic unit with an ~8 Ma depositional age overlies units with 12–10 Ma AHe ages, suggesting the possibility of an unconformity at the base of the conglomeratic interval, partially supported by the ~20° shallowing of dip reported for this unit [*Vergés et al*., 2001].

Despite the minor spread in AHe ages, comparison of all three sections reveals no significant age differences among localities. All samples except those from the upper Albarracín section have been reset, with AHe ages significantly younger (typically by 4–10 Myr) than the youngest U-Pb ages from the same sample. This indicates that the clastic sediments forming these sections must have been buried and heated to temperatures of 50–70°C in the period between deposition (~24–14 Ma) and subsequent exhumation. We hypothesize that this heating was related both to burial beneath additional basin fill (most of which has been subsequently removed) and to thrust sheet burial beneath nearby east vergent faults. Furthermore, when the AHe data from the three sections are combined (Figure 10), there emerges a strong signal at ~10 Ma of more than double the relative probability of other ages. We interpret this signal to be the peak exhumation age of the axial to eastern Precordillera.

6.3. Stratigraphic Trends

A comparison of mean AHe ages relative to stratigraphic position reveals ~12 Ma ages at the base and ~10 Ma ages near the top of each section, an unexpected but consistent trend of upsection younging of AHe ages. Potential explanations for the anomalous stratigraphic trend in AHe ages could involve factors that affected (1) compositional differences among apatite grains, (2) incomplete or irregular partial resetting, (3) geothermal gradients of the region, (4) localized heating near faults, or (5) nonuniform thrust burial histories.

1. Variations in apatite chemistry or the presence of inclusions or other imperfections could induce contrasting closure temperatures for individual grains and thus variable chronological results. However, there is no evidence for significant compositional, chemical, or grain size differences within individual successions (as demonstrated by the noncorrelation among AHe age, [eU], and spherical equivalent grain radius; Figure S2). Therefore, any variability is considered more likely to produce general scatter rather than the observed systematic trends.
2. An additional possibility is that individual grains were not fully reset and instead underwent systematic partial resetting that resulted in mean AHe ages that are shifted to progressively younger ages with respect to the true depositional ages represented by large populations of young zircons identified in U-Pb analyses (Figure 9). However, if this were the case, the highest samples should show no resetting and AHe ages should either coincide with depositional ages from corresponding stratigraphic levels (if the apatites are derived from young volcanic sources) or record a much older thermal history (if the apatites are derived from other sources)—a pattern not observed at Talacasto and Pachaco. Nevertheless, preliminary thermal histories generated by inverse modeling software (HeFTY) [*Ketcham*, 2005] capable of accommodating multiple samples reveal a potential alternative scenario in which some samples reach the 50–80°C window after 10 Ma, suggesting partial burial reheating of basin sediments.

3. Heat flow related to nearby coeval magmatism may affect AHe ages from selected areas in close proximity to these thermal anomalies. *Vergés et al*. [2001] proposed such igneous reheating for the Albarracín section. The distribution of Cenozoic igneous centers, however, suggests that such local resetting is unlikely to produce a consistent upsection shift in age patterns for all three basin segments.
4. Potential shear heating and/or geothermal fluid migration could promote excess heating of footwall basin fill within a few hundred meters of the bounding fault. Although we cannot conclusively rule out this option, we note that these localized effects would be comparable to the aforementioned process in which the hanging-wall overburden promoted longer heating of the proximal (western) footwall relative to the distal (eastern) footwall.
5. Finally, AHe age variations may result from uneven thrust burial in which upper deposits (along the western basin flanks) remain buried for a longer period because they are situated in the proximal (western) footwall, in close proximity to the adjacent thrust sheet. Durable rocks of the hanging-wall overburden remain atop younger basin fill for a longer period than older basin fill in distal eastern zones. Given the 1–2 km thickness of preserved basin fill, the time lag between cooling of the oldest (eastern) and youngest (western) basin fill in the footwall could be up to a few million years, depending on rates of erosion and fault displacement.

We favor this final option linking stratigraphic trends in AHe ages to variations in thrust burial (i.e., proximal versus distal footwall locations) and consider the differences in AHe ages within each section to be relatively minor. The limited age variation is particularly well represented in the context of the tight clustering of ages across all three sections (Figures 9 and 10). We consider the narrow range of AHe ages at a regional scale across different segments of the basin system to be fundamental in understanding the Precordillera exhumation history.

7. Discussion

Remnants of the Andean foreland basin system preserved in intermontane valleys of the Argentine Precordillera recorded sediment accumulation during initial hinterland shortening in the Frontal Cordillera, followed by later basin partitioning as deformation advanced eastward into the Precordillera thrust belt. By integrating depositional histories with geochronologic and thermochronologic data of clastic basin fill, we assess the timing of deformation and propose a middle to late Cenozoic reconstruction of a regional transect at 31–32°S (Figure 11).

Foreland basin development in this central segment of the Precordillera began at 24 Ma with the establishment of an incipient eolian system deposited unconformably on Devonian strata. An early Miocene shift from ephemeral playa lake conditions influenced by fluvial, volcanic, and eolian sedimentation to an extensive eolian system by 23–19 Ma is considered coeval with initial Andean shortening and uplift in the Frontal Cordillera. Roughly 21–14 Ma eolian sedimentation in the northern Precordillera [*Jordan et al*., 2001] confirms that eolian processes dominated a large foreland region during the early to middle Miocene.

By ~17 Ma, the foreland basin began recording well-organized fluvial sedimentation, with accumulation of gravel-sand braided stream deposits near the orogenic front and fine-grained floodplain deposits in distal eastern regions. The shift from eolian to fluvial sedimentation coincided with a change in detrital zircon U-Pb provenance. We propose that increased Late Permian and Triassic zircons in younger basin fill reflects a pulse of thrust-induced exhumation of the younger units of the Permo-Triassic Choiyoi Group. In the Frontal Cordillera, the spatial distribution of various Choiyoi units is related to Triassic extensional structures. At this time, the eastern block of the Frontal Cordillera (the Tocota horst) [*Heredia et al*., 2002] was elevated while western blocks were down dropped along normal faults. This resulted in heterogeneous preservation of younger Choiyoi units in the west and exposure of older Choiyoi units in the east. Therefore, the appearance of Upper Choiyoi zircons suggests that western blocks of the Frontal Cordillera were selectively uplifted and became the main source of foreland fluvial sediments (Figure 11b).

Earliest thrusting in the Precordillera may have started during early Miocene fluvial sedimentation. Evidence of initial erosion is preserved in upper Pachaco strata as a moderate proportion (20–30%) of Precordillera-derived Paleozoic age sandstone clasts within unit P3 (Figure 6) and as early Paleozoic and Mesoproterozoic zircon U-Pb age populations (sample PAU11 in Figure 7). These older signatures are absent in underlying eolian units, suggesting the zircons originated from a new source, most likely Paleozoic rocks brought to the surface by initial Precordillera deformation.

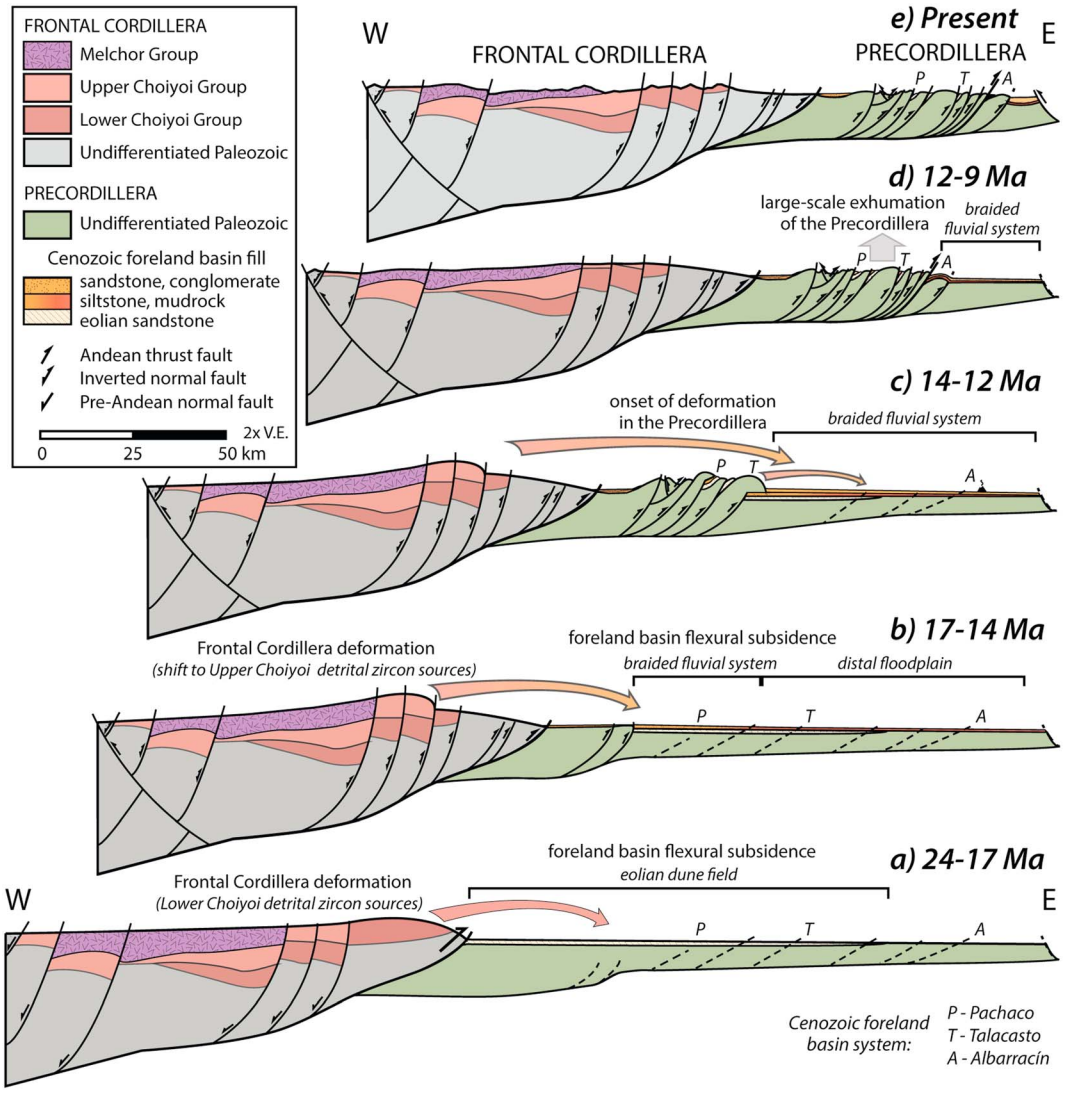

Figure 11. Proposed sequential restoration showing late Oligocene to present deformation of the Frontal Cordillera and Precordillera along with foreland basin evolution and fragmentation. Generalized cross sections are schematically represented for the Frontal Cordillera [after *Heredia et al*., 2002] and Precordillera [after *von Gosen*, 1992; *Kley et al*., 1999; *Cristallini and Ramos*, 2000; *Alonso*, 2005]. (a) 24–17 Ma: eolian sedimentation in foreland basin (units P1, P2, T1, and T2); broadly coeval initiation of thrusting in the Frontal Cordillera. (b) 17–14 Ma: main phase of thrusting in the Frontal Cordillera (reactivation of normal faults and activation of new thrusts) exposes Upper Choiyoi units; possible inception of thrusting in the westernmost Precordillera; foreland basin deposition of interbedded fluvial sandstones and conglomerates (unit P3, T3, and A3). (c) 14–12 Ma: development of thin-skinned thrust belt in the Precordillera, with structural partitioning of the once-contiguous foreland basin at Pachaco and Talacasto; Albarracín deposition of volcaniclastic unit A2 and interbedded sandstones and conglomerates of unit A3. (d) 12–9 Ma: rapid deformation and uplift of the Precordillera; additional burial then exhumation of Albarracín section. (e) 9 Ma to present: deformation front propagates eastward to easternmost Precordillera and Sierras Pampeanas; deposition then deformation of conglomeratic unit A4.

By 14 Ma, the Pachaco and Talacasto successions became segmented and buried by Paleozoic hanging-wall rocks carried by east directed thrust faults in the axial Precordillera. At this time, the Albarracín locality farther east was still undeformed, experiencing middle Miocene deposition of large volumes of pyroclastic material from nearby eruptive centers, followed by sand and gravel deposition in a braided fluvial system (Figure 11c).

Around 10 Ma, many segments of the Precordillera thrust belt and intervening panels of Cenozoic foreland basin fill experienced rapid, large-scale exhumation. The apatite (U-Th)/He ages of basin fill in the Pachaco, Talacasto, and Albarracín sections cluster between 12 and 9 Ma, despite their contrasting

locations across the thrust belt. Each section is exposed between different thrust sheets, and their original restored positions prior to shortening suggest an extensive E-W (strike-perpendicular) distribution over a distance of roughly 50–100 km (Figure 11a). Despite the earlier eastward propagation of deformation from the Frontal Cordillera to the western Precordillera, the ages of exhumational cooling across the axial to eastern Precordillera do not follow this sequential pattern. Rather, the tight clustering of AHe ages at 12–9 Ma across all three sections suggests focused contemporaneous exhumation over an extensive segment of the proximal foreland basin in the earliest late Miocene, likely due to synchronous thrusting above a single décollement linking multiple thrusts across the axial to eastern Precordillera.

The eastward advance of shortening from the Frontal Cordillera and abruptly across the central segment of the Precordillera at 31–32°S is relatively similar to the better-documented northern Precordillera at 28–30°S. Although shortening commenced earlier (at ~21–18 Ma) in the northern Precordillera, the main phase of deformation is similarly concentrated during the late Miocene [*Beer and Jordan*, 1989; *Jordan et al*., 1993, 1997, 2001]. Both the central and northern segments of the Precordillera record simultaneous displacement along multiple thrust faults at roughly 12–9 Ma, suggesting that the entire Precordillera thrust belt developed nearly synchronously along strike, with limited variation from north to south. This rapid and relatively uniform advance of thrusting toward the craton conflicts with the documented southward sweep of flat-slab subduction [*Kay et al*., 1991; *Yáñez et al*., 2001; *Ramos et al*., 2002] and highlights the potential importance of other influences beyond slab dip in influencing the kinematics of fold-thrust deformation in the Andes [e.g., *Allmendinger et al*., 1983; *Kley et al*., 1999].

8. Conclusions

1. Clastic depositional patterns are recorded in three intermontane exposures (Pachaco, Albarracín, and Talacasto) of the late Oligocene-Miocene retroarc foreland basin system in the central Precordillera of Argentina. The oldest strata record a ~24 Ma transition from ephemeral playa lake/incipient dune field conditions to a regional eolian system. By 17 Ma, the eolian system was replaced by sandy to gravelly braided fluvial sedimentation in the west (Pachaco section) and fine-grained floodplain deposition in the east (Talacasto and Albarracín). Upward coarsening fluvial and alluvial fan deposits reflect a 17–8 Ma shift from distal to proximal foreland basin facies, locally influenced by synorogenic volcanic activity. This pattern is consistent with an eastward (cratonward) progression of thin-skinned thrusting comparable to the northern segment of the Precordillera.
2. Shifts in conglomerate clast compositions record provenance variations attributable to uplift-induced exhumation of the Frontal Cordillera and subsequent development of the Precordillera thrust belt. Clast counts for the Pachaco section and uppermost Albarracín section are dominated by distal clasts from the Frontal Cordillera hinterland, with the remaining 20–30% from Silurian-Devonian units of the Precordillera. The proportion of Precordillera clasts greatly increases in the lower portion of the massive Albarracín conglomeratic unit, consistent with a pulse of sedimentation linked to nearby thrusting. Decreases in Precordillera clasts in the upper levels of this youngest unit suggest recycling of Frontal Cordillera clasts from newly uplifted basin fill or renewed contributions from western sources, potentially due to increased Frontal Cordillera uplift, diminished Precordillera shortening, or drainage reorganization.
3. Detrital zircon U-Pb ages reveal major contributions from the Andean arc, with distinct signatures related to unroofing of the Frontal Cordillera and initial exhumation of the Precordillera thrust belt. Age spectra are dominated by an abundance of Cenozoic volcanic grains, which show a systematic younging upsection, consistent with syndepositional volcanism. The U-Pb data constrain depositional ages of Pachaco and Talacasto basin fill from 24 to 14 Ma and allow for direct correlation between these sections. Depositional ages for the Albarracín section range from 17 to 8 Ma, recording an input of pyroclastic material from nearby eruptive centers. U-Pb results show a strong contribution of Permo-Triassic zircons from the Choiyoi Group, which composes the bulk of the Frontal Cordillera. A shift from an older to younger Choiyoi signal marks significant uplift within the Frontal Cordillera and is coincident with the ~17 Ma onset of fluvial sedimentation. U-Pb age populations also show Early Triassic and Mesoproterozoic zircons, which are present only in the youngest basin fill and indicative of initial widespread erosion of Precordillera thrust sheets.

4. Results from apatite helium thermochronometry record the timing of uplift-induced exhumation of Precordillera thrust sheets and overlying basin fill. Apatite (U-Th)/He ages show no systematic differences among the Talacasto, Pachaco, and Albarracín basin segments, and the majority fall in the 12–9 Ma range, with a strong pulse at ~10 Ma. These data suggest that the Precordillera thrust belt experienced rapid uplift and exhumational cooling in the late Miocene due to synchronous displacement on multiple thrusts linked to the regional décollement. Thus, the three intermontane segments represent a once-contiguous foreland basin broken by later thrusting rather than a series of isolated piggyback basins generated by syndepositional thrusting.
5. Sedimentologic and clast compositional data coupled with detrital zircon U-Pb and apatite (U-Th)/He results provide a foundation for linking basin evolution to regional thrusting. Intermontane remnants of Cenozoic basin fill within the central Precordillera recorded deposition in a broad foreland basin system during growth of the Frontal Cordillera to the west. Low-temperature thermochronometric results from these deposits preserve the subsequent initiation of shortening within the Precordillera thrust belt. Our field-based sedimentary observations, provenance data, and geochronologic and thermochronologic results are consistent with a laterally extensive foreland basin system that recorded uneven eastward advance of Oligocene to middle Miocene deformation and became sequentially partitioned during late Miocene construction of the axial to eastern Precordillera. We attribute final uplift and exhumation of studied basin segments to a large-scale regional event of rapid thrust propagation across the entire Precordillera at 12–9 Ma.

Acknowledgments
Funding was provided by student research grants (awarded to M.L.) from the Geological Society of America, American Association of Petroleum Geologists, and the Jackson School of Geosciences, as well as NSF grant EAR-1348031 and University of Texas Faculty Research Assignment (awarded to B.K.H.). We thank Patricia Alvarado, N. Ryan McKenzie, Sebastian Ramirez, and Julieta Ruiz for field assistance, logistical advice, and helpful discussions. Productive interactions with Kurt Constenius, Richard Ketcham, and Victor Ramos, as well as constructive reviews by Richard Allmendinger, Julie Fosdick, and Jeffrey Rahl, helped clarify the presentation.

References

Allmendinger, R. W., V. A. Ramos, T. E. Jordan, T. E. M. Palma, and B. L. Isacks (1983), Paleogeography and Andean structural geometry, northwest Argentina, *Tectonics*, *2*, 1–16, doi:10.1029/TC002i001p00001.

Allmendinger, R. W., D. Figueroa, D. Snyder, J. Beer, C. Mpodozis, and B. Isacks (1990), Foreland shortening and crustal balancing in the Andes at 30°S latitude, *Tectonics*, *9*(4), 789–809, doi:10.1029/TC009i004p00789.

Alonso, J. L., L. R. Rodríguez-Fernández, J. García-Sansegundo, N. Heredia, P. Farias, and J. Gallastegui (2005), Gondwanic and Andean structure in the Argentine central Precordillera: The Río San Juan section revisited, in *6th International Symposium on Andean Geodynamics*, pp. 36–39, IRD Editions, Paris.

Aparicio, E. P. (1969), Contribución al conocimiento de la edad de los sedimentos del arroyo de Agua Negra, Departamento de Iglesia, San Juan, República Argentina, *Rev. Asoc. Geol. Argent.*, *31*(3), 190–193.

Beer, J. A., and T. E. Jordan (1989), The effects of Neogene thrusting on deposition in the Bermejo Basin, Argentina, *J. Sediment. Petrol.*, *59*(2), 330–345, doi:10.1306/212F8F8A-2B24-11D7-8648000102C1865D.

Bercowski, F., and G. Figueroa (1987), Flujos piroclásticos en la Formación Albarracín, Terciario, Precordillera, San Juan, Argentina, in *XIII Congreso Geológico Argentino and III Congreso de Exploracion de Hidrocarburos*, vol. 4, pp. 225–227, Asoc. Geol. Argent., Buenos Aires.

Cahill, T., and B. L. Isacks (1992), Seismicity and shape of the subducted Nazca plate, *J. Geophys. Res.*, *97*(B12), 17,503–17,529, doi:10.1029/92JB00493.

Cristallini, E. O., and V. A. Ramos (2000), Thick-skinned and thin-skinned thrusting in the La Ramada fold and thrust belt: Crustal evolution of the High Andes of San Juan, Argentina (32°SL), *Tectonophysics*, *317*(3-4), 205–235, doi:10.1016/S0040-1951(99)00276-0.

Dahlquist, J. A., R. J. Pankhurst, C. W. Rapela, C. Galindo, P. Alasino, C. M. Fanning, J. Saavedra, and E. Baldo (2008), New SHRIMP U-Pb data from the Famatina Complex: Constraining Early – Mid Ordovician Famatinian magmatism in the Sierras Pampeanas, Argentina, *Geol. Acta*, *6*(4), 319–333, doi:10.1344/105.000000260.

Damanti, J. F. (1993), Geomorphic and structural controls on facies patterns and sediment composition in a modern foreland basin, in *Alluvial Sedimentation*, *Spec. Publ. Int. Assoc. Sedimentol.*, vol. 17, edited by M. Marzo and C. Puigdefábregas, pp. 221–233, Blackwell, Oxford, U. K., doi:10.1002/9781444303995.ch17.

Echavarria, L., R. Hernández, R. Allmendinger, and J. Reynolds (2003), Subandean thrust and fold belt of northwestern Argentina: Geometry and timing of the Andean evolution, *AAPG Bull.*, *87*, 965–985.

Ehlers, T. A., and K. A. Farley (2003), Apatite (U–Th)/He thermochronometry: Methods and applications to problems in tectonic and surface processes, *Earth Planet. Sci. Lett.*, *206*, 1–14.

Farley, K. A. (2000), Helium diffusion from apatite: General behavior as illustrated by Durango fluorapatite, *J. Geophys. Res.*, *105*(B2), 2903–2914, doi:10.1029/1999JB900348.

Farley, K. A. (2002), (U-Th)/He dating: Techniques, calibrations, and applications, *Rev. Mineral. Geochem.*, *47*(1), 819–844, doi:10.2138/rmg.2002.47.18.

Farley, K. A., and D. F. Stockli (2002), (U-Th)/He dating of phosphates: Apatite, monazite, and xenotime, *Rev. Mineral. Geochem.*, *48*(1), 559–577, doi:10.2138/rmg.2002.48.15.

Farley, K. A., R. A. Wolf, and L. T. Silver (1996), The effects of long alpha-stopping distances on (U-Th)/He ages, *Geochim. Cosmochim. Acta*, *60*(21), 4223–4229.

Finney, S., S. H. Peralta, G. Gehrels, and K. Marsaglia (2005), The Early Paleozoic history of the Cuyania (greater Precordillera) terrane of western Argentina: Evidence from geochronology of detrital zircons from Middle Cambrian sandstones, *Geol. Acta*, *3*(4), 339–354.

Flowers, R. M., R. A. Ketcham, D. L. Shuster, and K. A. Farley (2009), Apatite (U–Th)/He thermochronometry using a radiation damage accumulation and annealing model, *Geochim. Cosmochim. Acta*, *73*(8), 2347–2365, doi:10.1016/j.gca.2009.01.015.

Giambiagi, L. B., and A. N. Martinez (2008), Permo-Triassic oblique extension in the Potrerillos-Uspallata area, western Argentina, *J. South Am. Earth Sci.*, *26*(3), 252–260, doi:10.1016/j.jsames.2008.08.008.

Grosse, P., F. Söllner, M. A. Báez, A. I. Toselli, J. N. Rossi, and J. D. de la Rosa (2009), Lower Carboniferous post-orogenic granites in central-eastern Sierra de Velasco, Sierras Pampeanas, Argentina: U–Pb monazite geochronology, geochemistry and Sr–Nd isotopes, *Int. J. Earth Sci.*, *98*(5), 1001–1025, doi:10.1007/s00531-007-0297-5.

Guion, P. D. (1984), Crevasse splay deposits and roof-rock quality in the Threequarters Seam (Carboniferous) in the East Midlands Coalfield, UK, in *Sedimentology of Coal and Coal-Bearing Sequences*, *Spec. Publ. Int. Assoc. Sedimentol.*, vol. 7, edited by R. A. Rahmani and R. M. Flores, pp. 291–308, Blackwell, Oxford, U. K., doi:10.1002/9781444303797.ch16.

Heredia, N., L. R. Rodriguez Fernández, G. Gallastegui, P. Busquets, and F. Colombo (2002), Geological setting of the Argentine Frontal Cordillera in the flat-slab segment (30°00′–31°30′S latitude), *J. South Am. Earth Sci.*, *15*, 79–99.

Horton, B. K. (1998), Sediment accumulation on top of the Andean orogenic wedge: Oligocene to late Miocene basins of the Eastern Cordillera, southern Bolivia, *Geol. Soc. Am. Bull.*, *110*, 1174–1192.

Horton, B. K. (2005), Revised deformation history of the central Andes: Inferences from Cenozoic foredeep and intermontane basins of the Eastern Cordillera, Bolivia, *Tectonics*, *24*, TC3011, doi:10.1029/2003TC001619.

Howard, J. L. (1993), The statistics of counting clasts in rudites: A review, with examples from the upper Palaeogene of southern California, USA, *Sedimentology*, *40*(2), 157–174, doi:10.1111/j.1365-3091.1993.tb01759.x.

Irigoyen, M. V., K. L. Buchan, and R. L. Brown (2000), Magnetostratigraphy of Neogene Andean foreland-basin strata, lat 33°S, Mendoza Province, Argentina, *Geol. Soc. Am. Bull.*, *112*, 803–816.

Johnson, N. M., T. E. Jordan, P. A. Johnsson, and C. W. Naeser (1986), Magnetic polarity stratigraphy, age and tectonic setting of fluvial sediments in the eastern Andean foreland basin, San Juan province, Argentina, *Int. Assoc. Sedimentol., Spec. Publ, 8*, 63–75.

Jordan, T. E. (1995), Retroarc foreland and related basins, in *Tectonics of Sedimentary Basins*, edited by C. Busby and R. Ingersoll, pp. 331–362, Blackwell Scientific Publications, Oxford, U. K.

Jordan, T. E., and R. N. Alonso (1987), Cenozoic stratigraphy and basin tectonics of the Andes Mountains, 20°–28° south latitude, *Am. Assoc. Pet. Geol. Bull.*, *71*, 49–64.

Jordan, T. E., B. L. Isacks, R. W. Allmendinger, J. A. Brewer, V. A. Ramos, and C. J. Ando (1983), Andean tectonics related to geometry of subducted Nazca plate, *Geol. Soc. Am. Bull.*, *94*(3), 341–361, doi:10.1130/0016-7606(1983)94<341.

Jordan, T. E., R. W. Allmendinger, J. F. Damanti, and R. E. Drake (1993), Chronology of motion in a complete thrust belt: The Precordillera, 30–31°S, Andes Mountains, *J. Geol.*, *101*(2), 135–156.

Jordan, T. E., J. H. Reynolds, and J. P. Erikson (1997), Variability in age of initial shortening and uplift in the central Andes, 16–33°30′S, in *Tectonic Uplift and Climate Change*, edited by W. F. Ruddiman, pp. 41–61, Plenum, New York.

Jordan, T. E., F. Schlunegger, and N. Cardozo (2001), Unsteady and spatially variable evolution of the Neogene Andean Bermejo foreland basin, Argentina, *J. South Am. Earth Sci.*, *14*(7), 775–798, doi:10.1016/S0895-9811(01)00072-4.

Kay, S. M., and J. M. Abbruzzi (1996), Magmatic evidence for Neogene lithospheric evolution of the central Andean "flat-slab" between 30°S and 32°S, *Tectonophysics*, *259*(1-3), 15–28, doi:10.1016/0040-1951(96)00032-7.

Kay, S. M., and C. Mpodozis (2002), Magmatism as a probe to the Neogene shallowing of the Nazca plate beneath the modern Chilean flat-slab, *J. South Am. Earth Sci.*, *15*, 39–57.

Kay, S. M., V. Maksaev, R. Moscoso, C. Mpodozis, C. Nasi, and C. E. Gordillo (1988), Tertiary Andean magmatism in Chile and Argentina between 28°S and 33°S: Correlation of magmatic chemistry with a changing Benioff zone, *J. South Am. Earth Sci.*, *1*(1), 21–38, doi:10.1016/0895-9811(88)90013-2.

Kay, S. M., C. Mpodozis, V. A. Ramos, and F. Munizaga (1991), Magma source variations for mid–late Tertiary magmatic rocks associated with a shallowing subduction zone and a thickening crust in the Central Andes (28–33°S), in *Andean Magmatism and its Tectonic Setting*, edited by R. S. Harmon and C. W. Rapela, *Geol. Soc. Am. Spec. Pap.*, *265*, 113–138.

Ketcham, R. A. (2005), Forward and inverse modeling of low-temperature thermochronometry data, *Rev. Min. Geochem.*, *58*(1), 275–314, doi:10.2138/rmg.2005.58.11.

Kley, J., C. R. Monaldi, and J. A. Salfity (1999), Along-strike segmentation of the Andean foreland: Causes and consequences, *Tectonophysics*, *301*(1-2), 75–94, doi:10.1016/S0040-1951(98)90223-2.

Langford, R. P., and M. A. Chan (1989), Fluvial-aeolian interactions: Part II. Ancient systems, *Sedimentology*, *36*, 1037–1051.

Leveratto, M. A. (1968), Geología del oeste de Ullúm-Zonda, borde oriental de la Precordillera de San Juan, *Rev. Asoc. Geol. Argent.*, *23*(2), 129–157.

López-Gamundí, O. R., and R. A. Astini (2004), Alluvial fan–lacustrine association in the fault tip end of a half-graben, northern Triassic Cuyo basin, western Argentina, *J. South Am. Earth Sci.*, *17*(4), 253–265, doi:10.1016/j.jsames.2004.06.004.

Miall, A. D. (1996), *The Geology of Fluvial Deposits*, Springer, Berlin.

Milana, J. P. (1993), Estratigrafía de eolianitas en la zona de Jáchal-Huaco, Precordillera de San Juan, *Rev. Asoc. Geol. Argent.*, *48*(3-4), 283–298.

Milana, J. P., M. F. Cevallos, A. M. Zavatierri, M. Prampano, and H. O. Papu (1993), La sequencia terciaria de Pachaco: Sedimentologia, edad, corellaciones y significado paleogeografico, in *XII Congreso Geológico Argentino y II Congreso de Exploracion de Hidrocarburos*, vol. 1, pp. 226–234, Asoc. Geol. Argent., Buenos Aires.

Milana, J. P., F. Bercowski, and T. Jordan (2003), Paleoambientes y magnetoestratigrafía del Neógeno de la Sierra de Mogna, y su relación con la Cuenca de Antepaís Andina, *Rev. Asoc. Geol. Argent.*, *58*(3), 447–473.

Pankhurst, R. J., C. W. Rapela, and C. M. Fanning (2000), Age and origin of coeval TTG, I- and S-type granites in the Famatinian belt of NW Argentina, *Trans. R. Soc. Edinburgh: Earth Sci.*, *91*(1-2), 151–168.

Pardo-Casas, F., and P. Molnar (1987), Relative motion of the Nazca (Farallon) and South American plates since Late Cretaceous time, *Tectonics*, *6*(3), 223–248, doi:10.1029/TC006i003p00233.

Persano, C., D. N. Barfod, F. M. Stuart, and P. Bishop (2007), Constraints on early Cenozoic underplating-driven uplift and denudation of western Scotland from low temperature thermochronometry, *Earth Planet. Sci. Lett.*, *263*(3-4), 404–419, doi:10.1016/j.epsl.2007.09.016.

Polanski, J. (1970), *Carbónico y Pérmico de la Argentina*, pp. 216, Eudeba, Buenos Aires.

Rahl, J. M., T. A. Ehlers, and B. A. van der Pluijm (2007), Quantifying transient erosion of orogens with detrital thermochronology from syntectonic basin deposits, *Earth Planet. Sci. Lett.*, *256*(1-2), 147–161.

Ramos, V. A. (1995), Field guide to the geology of Precordillera folded and thrust belt (Central Andes), ICL-COMTEC-AGA, 64.

Ramos, V. A. (1999), Los depósitos sinorogénicos terciarios de la región andina, in *Geología Argentina*, vol. 29, edited by R. Caminos, pp. 651–691, Inst. Geol. Recur. Miner., Buenos Aires.

Ramos, V. A. (2009), Anatomy and global context of the Andes: Main geologic features and the Andean orogenic cycle, *Geol. Soc. Am. Mem.*, *204*, 31–65, doi:10.1130/2009.1204(02).

Ramos, V. A., and A. Folguera (2009), Andean flat-slab subduction through time, *Geol. Soc. London, Spec. Publ.*, *327*(1), 31–54, doi:10.1144/SP327.3.

Ramos, V. A., and S. M. Kay (1991), Triassic rifting and associated basalts in the Cuyo basin, central Argentina, in *Andean Magmatism and its Tectonic Setting*, edited by R. S. Harmon and C. W. Rapela, *Geol. Soc. Am. Spec. Pap.*, *265*, 79–91.

Ramos, V. A., T. E. Jordan, and R. W. Allmendinger (1986), Paleozoic terranes of the central Argentine-Chilean Andes, *Tectonics*, *5*(6), 855–880, doi:10.1029/TC005i006p00855.

Ramos, V. A., E. O. Cristallini, and D. J. Perez (2002), The Pampean flat-slab of the Central Andes, *J. South Am. Earth Sci.*, *15*, 59–78.

Reiners, P. W., and K. A. Farley (2001), Influence of crystal size on apatite (U–Th)/He thermochronology: An example from the Bighorn Mountains, Wyoming, *Earth Planet. Sci. Lett.*, *188*, 413–420.
Rocha-Campos, A. C., M. A. Basei, A. P. Nutman, L. E. Kleiman, R. Varela, E. Llambias, F. M. Canile, and O. d. C. R. da Rosa (2011), 30 million years of Permian volcanism recorded in the Choiyoi igneous province (W Argentina) and their source for younger ash fall deposits in the Paraná Basin: SHRIMP U-Pb zircon geochronology evidence, *Gondwana Res.*, *19*, 509–523, doi:10.1016/j.palaeo.2010.09.001.
Shuster, D. L., R. M. Flowers, and K. A. Farley (2006), The influence of natural radiation damage on helium diffusion kinetics in apatite, *Earth Planet. Sci. Lett.*, *249*(3-4), 148–161, doi:10.1016/j.epsl.2006.07.028.
Siks, B. C., and B. K. Horton (2011), Growth and fragmentation of the Andean foreland basin during eastward advance of fold-thrust deformation, Puna plateau and Eastern Cordillera, northern Argentina, *Tectonics*, *30*, TC6017, doi:10.1029/2011TC002944.
Vergés, J., E. Ramos, D. Seward, P. Busquets, and F. Colombo (2001), Miocene sedimentary and tectonic evolution of the Andean Precordillera at 31 S, Argentina, *J. South Am. Earth Sci.*, *14*, 735–750.
Vergés, J., V. A. Ramos, A. Meigs, E. Cristallini, F. H. Bettini, and J. M. Cortes (2007), Crustal wedging triggering recent deformation in the Andean thrust front between 31°S and 33°S: Sierras Pampeanas-Precordillera interaction, *J. Geophys. Res.*, *112*, 1–22, doi:10.1029/2006JB004287.
Vermeesch, P. (2008), Three new ways to calculate average (U–Th)/He ages, *Chem. Geol.*, *249*(3-4), 339–347, doi:10.1016/j.chemgeo.2008.01.027.
Von Gosen, W. (1992), Structural evolution of the Argentine Precordillera: The Río San Juan section, *J. Struct. Geol.*, *14*(6), 643–667.
Yáñez, G. A., C. R. Ranero, R. von Huene, and J. Diaz (2001), Magnetic anomaly interpretation across the southern central Andes (32°–34°S): The role of the Juan Fernández Ridge in the late Tertiary evolution of the margin, *J. Geophys. Res.*, *106*(B4), 6325–6345, doi:10.1029/2000JB900337.
Zapata, T. R., and R. W. Allmendinger (1996a), Growth stratal records of instantaneous and progressive limb rotation in the Precordillera thrust belt and Bermejo basin, Argentina, *Tectonics*, *15*(5), 1065–1083, doi:10.1029/96TC00431.
Zapata, T. R., and R. W. Allmendinger (1996b), Thrust-front zone of the Precordillera, Argentina: A thick-skinned triangle zone, *AAPG Bull.*, *80*(3), 359–381.